End-Member Modelling Analysis (EMMA) applied to lavas cooled in high magnetic fields, Iceland and New-Zealand

Romy Meyer

July 2021

Supervised by Lennart de Groot

Abstract

Despite recent improved methods, obtaining paleointensities from lavas is still a complicated process. With the IZZI-Thellier method, samples are heated which makes them prone to (chemical) alteration, and success rates are often low. The pseudo-Thellier method avoids heating the samples but uses alternating fields to replace the natural remanent magnetization (NRM) of a sample with an anhysteretic remanent magnetization (ARM). However, the resulting calibration relationship which converts the pseudo-Thellier slope to a paleointensity, misses the origin. Also, various samples can not be used because their $B_{1/2ARM}$, a grain size selection criteria, is outside the accepted boundaries of 23 to 63mT. These and other previous paleointensity techniques assume all grains in a sample behave in a similar manner as they did when they acquired their NRM during cooling. The newly proposed End-Member Modelling Analysis (EMMA) avoids making grain size selections and assumes the magnetic remanence in a sample is carried by an assemblage of iron-oxides. Each one has their own mapping factor between the NRM acquired during cooling in a natural field and the ARM acquired in a laboratory field. The EMMA-model was previously capable of calculating accurate results for a real dataset with data from Hawaii and Reunion of which the paleointensity was known. They cover a small range of paleointensities from 35 to 40μT. Here I expand this calibration dataset with new data from recent lava flows of Iceland and New-Zealand, which cooled in fields of >50μT. The samples from these locations are subjected to all three paleointensity methods, and to a rock-magnetic study to identify the magnetic remanence carriers of the samples. The IZZI-Thellier method was very successful and confirms the assumed high paleointensities of the samples. The pseudo-Thellier method gave almost no results. The $B_{1/2ARM}$ of Iceland was too low, and of New-Zealand too high for most samples to be interpreted and for most other results the calibration relation calculated lower paleointensities than expected. The most accurate EMMA-model was based on a 3 end-member model with outliers, overprints and unsuccessful locations removed and ultimately contained 189 samples from Hawaii, Reunion, Tenerife, Iceland and New-Zealand. It calculated an average difference in paleointensity of -0.056μT and an absolute difference in paleointensity of 6.497μT. The successful samples had a $B_{1/2ARM}$ ranging from 16.3 to 124.7 mT which is a much wider range than would be selected with the pseudo-Thellier method. The three different end-members which the model determines for each sample seem to correlate to different Curie temperatures, which indicates the end-members are based on specific iron-oxide compositions. Future studies should expand the dataset further with more samples from high and low magnetic fields, with different types of compositions and therefore different possible end-members. A larger dataset could also

shed light on why some locations are unsuccessful and how to remove bad measurements from the dataset. Then the EMMA-model can be applied to sites for which the reference paleointensity is not known to improve future geomagnetic field models.

Contents

1 Introduction

The direction and intensity of the Earth's magnetic field is constantly changing in both time and space (Tauxe, 2010). These variations in the Earth's magnetic field are described by geomagnetic field models. These models are used for studies on space weather, to describe the dynamics of the Earth's core, and the Earth's magnetic field provides a source for navigation (Thébault et al., 2015). Direct measurements of the Earth's magnetic field are e.g. done using satellites and observatories, but these are only quite recent because the study of paleomagnetism originated around the mid-nineteenth century (Dunlop and Özdemir, 2001). To obtain older data prior to direct observations, scientists rely on baked archaeological artefacts and igneous rocks. Because the first is constrained to old civilisations at specific moments in time, the latter one is preferred because lavas can span a wide range of cooling ages. Therefore, changes in the present day Earth's magnetic field are well defined, but the evolution of the field and changes in for example geomagnetic lows are still poorly constrained. Furthermore, geomagnetic field models are overrepresented in data from the Northern Hemisphere and the models have a more limited amount of paleointensity data compared to directional data especially further back in time (Korte et al., 2011). This because it is rather straightforward to determine the direction of the field lines but obtaining reliable information about the paleointensity of the Earth's magnetic field is much more difficult.

To date, several techniques have been proposed to recover the paleointensity of rocks. The classical approach of Thellier (1959) was to heat a sample in several steps, whereby the natural remanent magnetization (NRM) acquired during cooling in the Earth's magnetic field was progressively replaced by partial thermal remanent magnetizations (pTRMs) in a laboratory field. However, because the samples are heated they are prone to (chemical) alteration or even the domain state of the specimens may change entirely (De Groot et al., 2014), which causes only 10-20% (Valet et al., 2010) of these classical Thellier style experiments to be reliable. Other techniques proposed are among others the IZZI-Thellier method (Tauxe and Staudigel, 2004), the microwave approach (Hill and Shaw, 1999), the multispecimen (MSP) technique (Dekkers and Böhnel, 2006) and the domain state corrected multispecimen technique (DSC-MSP) (Fabian and Leonhardt, 2010). The success rates of these techniques vary per study, ranging from ∼16%(MSP-DSC) to ∼32% (IZZI) (de Groot et al., 2015), which is still rather low.

Tauxe et al. (1995) presented a new method to extract relative paleointensity data from sediments, the pseudo-Thellier technique. Here, the NRM of a sample is removed using alternating fields (AF demagnetization). After demagnetization a DC-field is superimposed on the alternating field, replacing the NRM of the samples by an anhysteretic remanent magnetization (ARM) in the laboratory field during the same AF steps. This method therefore avoids heating the samples entirely. However, there is an unknown mapping factor between the naturally imparted NRMs and the laboratory imparted ARMs. Yu et al. (2003), who tested this method on lavas, showed that the ratio of TRM (thermal remanent magnetization) to ARM is strongly grain size dependent. De Groot et al. (2013) further developed the pseudo-Thellier approach with lavas from Hawaii and applied a grain size selection criterion named $B_{1/2ARM}$, which is the magnitude of the alternating field for which half of the maximum ARM was imparted. When the $B_{1/2ARM}$ is low, the sample responds quickly to an alternating field, when it is high the sample responds slowly to an alternating field. De Groot et al., 2013 found that the paleointensity of samples with a $B_{1/2ARM}$ between 23 and 63mT can be reliably used. They calculated a calibration equation to convert the slopes of the pseudo-Thellier approach to an absolute intensity value. De Groot et al. (2015,2016) updated this calibrated pseudo-Thellier technique by adding data from more locations. In these pseudo-Thellier slope against paleointensity plots (most recent one: Figure 1) the linear calibration relationship misses the origin. When the pseudo-Thellier slope is zero, it will give a paleointensity of at least 14.6μT. This is theoretically impossible because when a rock cools in a 14μT field, it will have a magnetization. De Groot et al., 2013 explains the non-zero y-axis as resulting from non-linear behavior for the calibration in the low field intensities area, but could not solve this issue.

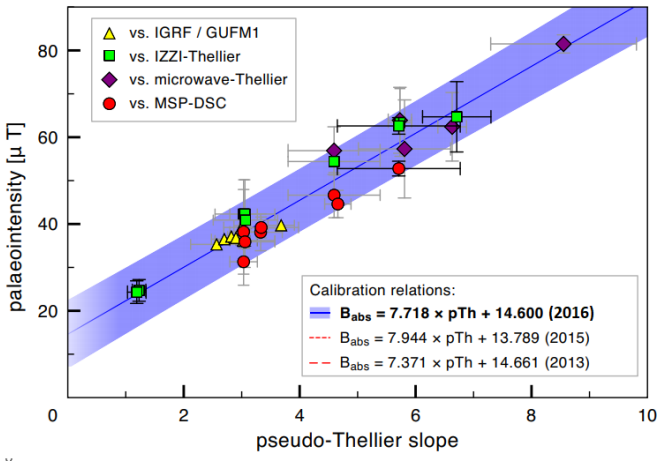

Figure 1: The calibrated pseudo-Thellier plot from De Groot et al. (2016), with data from De Groot et al. (2013,2015) where the pseudo-Thellier results are plotted against the paleointensities according to field models or other paleointensity experiment data. The calibration relation misses the origin.

All paleointensity techniques, including the IZZI-Thellier and pseudo-Thellier method, assume all grains in a sample in the lab behave in a similar manner as they did when they acquired their NRM during cooling. However, the magnetic remanence in lavas is carried by an assemblage of iron-oxides, such as magnetite and hematite, with many different grain sizes, shapes and compositions. Magnetite occurs in the magnetite (Fe_3O_4)-ulvöspinel(Fe_2TiO_4) solid solution, whereby titanium ions substitute for iron in the crystal structure. Pure magnetite has no titanium, with increasing titanium replacement the minerals are named titanomagnetites (TMx, the x stands for amount of titanium content). The amount of titanium affects the magnetic properties of a sample. For example, with increasing amounts of titanium the Curie temperature drops. Magnetite has a Curie temperature of 578°C and ulvöspinel a Néel temperature of -153°C (Putnis, 1992, Figure 2).

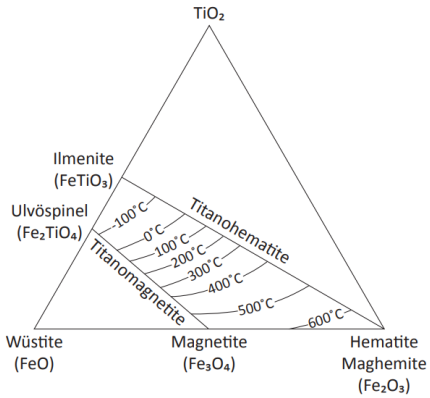

Figure 2: Ternary diagram illustrating the ulvöspinel-magnetite solid solution series with increasing Curie temperature, and the ilmenite-hematite solid solution. From Readman and O'reilly (1972)

The previous calibrated pseudo-Thellier technique of De Groot et al. (2013,2016) did not take this distribution of iron-oxides into account, but worked somewhat because their grain-size selection excluded some samples to get a more homogeneous iron-oxide distribution in the sample set. Recently an end-member model of the calibrated pseudo-Thellier technique was proposed, the end-member modelling analysis (EMMA) technique. It unmixes the NRM demagnetization and the ARM acquisition curves into end-members (Liz van Grinsven, Guided Research) that might represent iron-oxides with different properties.

The idea of the EMMA technique is that each sample consists of different grains with a different distribution of minerals. The bulk measurement of a sample is the sum of the contributions from all these grains. Each end-member has its own mapping factor between the original NRM and the laboratory acquired ARM. With the EMMA-model it is possible to acquire this mapping factor when the field in which the sample cooled is known, however, in most paleointensity studies this is exactly the unknown data which you want to calculate.

To be able to calculate paleointensities, first the mapping relation of the different end-members is to be determined. Therefore, we need a wide range of volcanic rocks that vary in composition and that cooled in different known Earth magnetic field strengths (Liz van Grinsven, GR). With such a calibration dataset we cover a wide range of possible mapping relations. The model was previously tested on a computational and real data-set. The real data set consists of samples from Hawaii and Reunion, data from Etna, Iceland and Tenerife were unsuccessful in this model. The known paleofields covered at Hawaii and Reunion are almost similar and range from 35μT to 40μT. To expand the calibration dataset, samples from regions where the lavaflows cooled in high and low magnetic fields are needed. In this study samples from Iceland and New-Zealand, which cooled in fields $>50\mu$T, are subjected to the EMMA-approach. First the magnetic remanence carriers in the samples are identified with rock magnetic analyses. Then, IZZI-Thellier and calibrated pseudo-Thellier techniques are applied to the samples to check whether the expected paleointensities are found with these techniques and observe the success rate of these methods. Lastly, the end-member model is applied to expand the calibration dataset with samples from Iceland and New-Zealand. Eventually, the EMMA-approach may be applied to calculate paleointensities of samples with unknown fields, to improve future geomagnetic field models.

2 Geological settings

The locations sampled in this study are Iceland and New-Zealand, which are two very different regions. Some geological background is given for both, as well as the age of the lava flows and the location of the sites which were sampled. Most samples come from young lavaflows, of which the strength of the Earths magnetic field at the time of eruption is known. Therefore both locations are ideal for this study.

2.1 Iceland

Iceland is located at the Mid-Atlantic ridge, the spreading ridge separating the North American and Eurasian plates, with a stationary hot spot beneath it. Active volcanism results from these two features, and volcanic activity in Iceland is divided into several zones (Figure 3), the Northern (NVZ) and Western Volcanic Zones (WVZ) are the axial zone and point of active spreading characterised by tholeiitic magmatism. The Eastern Volcanic Zone (EVZ) is a developing axial rift also dominated by tholeiitic magmatism but with mildly alkalic magmatism, that eventually will take over from the WVZ (Thordarson and Larsen, 2007). The EVZ is the most active region, giving the largest contribution of the volume of erupted magma (Thordarson and Larsen, 2007). Part of the Eastern Volcanic Zone is the Hekla stratovolcano, which is the second most active volcano in Iceland. It erupted several times since the first well documented eruption in 1947 (Höskuldsson et al., 2007). The composition of the lava ranges from dacite to basaltic andesite (Thordarson and

Larsen, 2007).

During a field trip in 2016 several loose blocks were gathered from different recent flows of the Hekla volcano. Paleomagnetic cores were drilled from these blocks once back in Utrecht. Therefore, the samples were not orientated with respect to the (magnetic) north. The blocks were taken from eight different sites (Figure 2, Table 1). Samples IL-08 and IL-09 are from approximately the same site, but the two different lava flows could be distinguished in the field due to color differences and different level to each other. Site IL-02 should be from the 1980 flow but the location is slightly next to the flow identified by Pedersen et al. (2018).

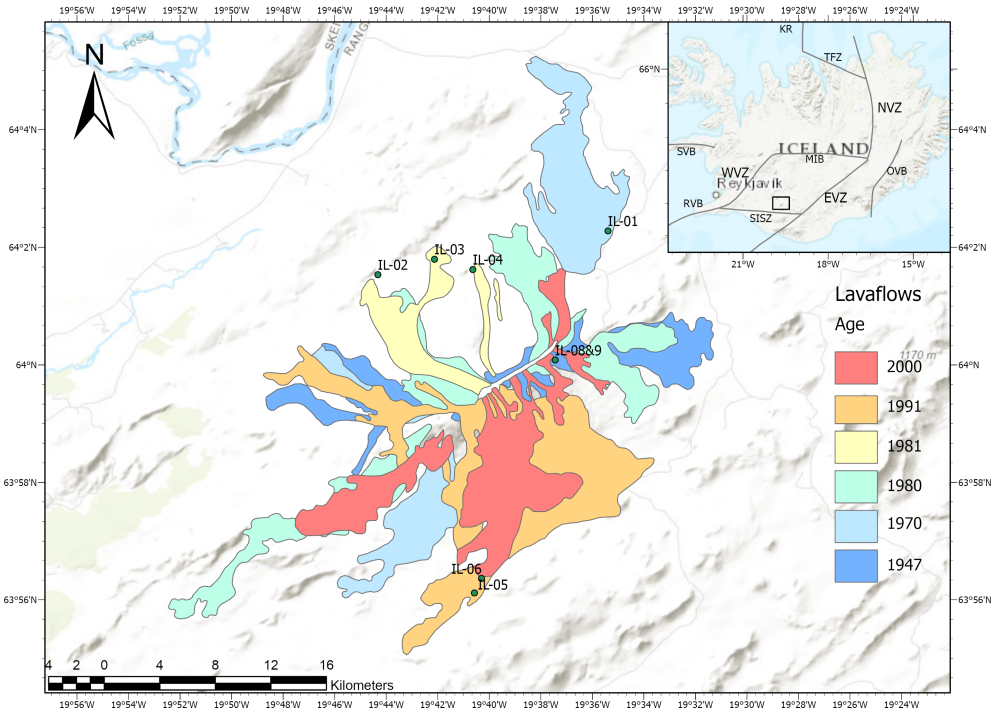

Figure 3: Map of the Hekla volcano, Iceland, showing the location of lavaflows from eruptions of 1947 to 2000. Green dots are the sites sampled for this study. EVZ: East Volcanic Zone, NVZ: North Volcanic Zone, WVZ: West Volcanic Zone, MIB: Mid-Iceland Belt, SVB:Snaefellsnes Volcanic Belt, OVB: Oraefi Volcanic Belt, KR: Kolbeinsey Ridge, TFZ: Tjörnes Fracture Zone, SISZ: South Iceland Seismic Zone. Location of the lavaflows are from Pedersen et al. (2018), location of the volcanic zones are from Thordarson and Larsen (2007)

Table 1: Site details Iceland

Site name		Coordinates	Flow age	Href(μT)	Remark
IL-01	64.037972	-19.589882	1970	51.63	
IL-02	64.025582	-19.738765	1980	51.92	Site location next to flow (see map)
IL-03	64.029971	-19.702106	1981	51.92	
IL-04	64.027062	-19.677339	1981	51.92	
IL-05	63.935223	-19.676308	1991	51.92	
IL-06	63.939347	-19.671669	2000	51.92	
IL-08	64.001374	-19.624075	1980	51.92	IL-08 flow in contact with IL-09
IL-09	64.001374	-19.624075	2000	52.00	IL-09 flow in contact with IL-08

Given are the site names, coordinates of the sampling locations, age of the flows, the reference IGRF (2019) field values (Href) and possible remarks

2.2 New-Zealand

The North Island of New-Zealand is composed of several volcanoes, which are located in the Taupo Volcanic Zone. Volcanism is in a backarc setting and has been active since around 2Ma (Wilson et al., 1984), due to the subduction of the Pacific plate beneath the Northern Island (Miller and Williams-Jones, 2016). Part of the Taupo Volcanic Zone is the Tongariro Volcanic Complex, which erupted first around 273ka (Hobden et al., 1996). Mt. Ngauruhoe is a frequently active composite cone of Mt. Tongariro and the youngest of at least nine cones. Its activity started around 2.5ka and it has grown over older Tongariro cones, covering an area of 15km2 and reaching a height of 900m, 2.287m above sea level (Hobden et al., 2002). Mt. Ngauruhoe erupt basaltic andesite to andesite a'a-type lava flows of which the most recent eruptions were in 1954, 1974 and 1975 (Hobden et al., 2002).

During a fieldtrip several blocks were collected from the NW-flanks of Mt. Ngauruhoe (Figure 4). A few samples were oriented with respect to the magnetic north by a marked strike and dip on a relatively flat surface, which was rather difficult due to the irregular surface of the lava flow. For the other samples the cores are oriented relatively to each other. The samples were sent to Utrecht University, with a sample summary describing the characteristics and locations of the sites. The names, locations and (if known) ages of the sites are shown in Table 2. The exact location of site NZ-04 is unknown, except that at least NZ-04-3 and NZ-04-4 are from the 1954 flow. Sites NZ-04-1 and NZ-04-2 were sampled in between the 1954 flows and possibly of historic age and therefore their reference paleointensity in uncertain. Sites NZ-02 and NZ-03 were according to the sample summary from a 1954 flow, but according to their coordinates compared to location of flows from Hobden et al. (2002), they are from an 1870 flow. Because the reference paleointensity in 1870 is not far off the paleointensity at 1954 (around 57μT), the assumption and interpretation of the sample summary is kept in Table 2.

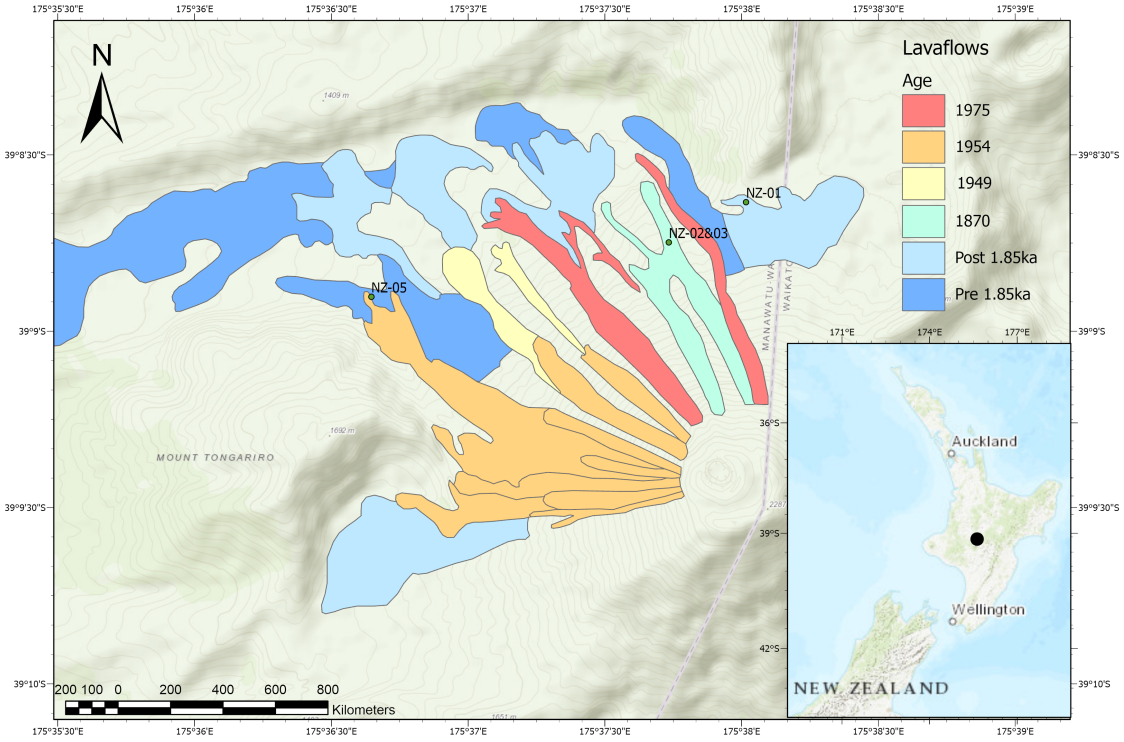

Figure 4: Map of the NW-side of Mt. Ngauruhoe, New-Zealand, showing the location of lavaflows of various eruptions, of pre-historical age to the eruption of 1975. Green dots are the sites sampled for this study. The location of site NZ-04 is unclear, NZ-04-1&2 are in between the 1954' flows and possible of pre-historical age, NZ-04-3&4 are immediately adjacent to NZ-04-1&2 but for certain from the 1954 flow. Location of the lavaflows are from Hobden et al. (2002).

Table 2: Site details New-Zealand

Site name		Coordinates	Flow age	Href(μT)	Remark
NZ-01	-39.143902	175.633602	Post 1.85ka	??	
NZ-02	-39.145811	175.628896	1954	56.86	
NZ-03	-39.145811	175.628896	1954	56.86	
NZ-04-1	??	??	Historic	??	Blocks inbetween 1954' flows
NZ-04-2	??	??	Historic	??	Blocks inbetween 1954' flows
NZ-04-3	??	??	1954	56.86	
NZ-04-4	??	??	1954	56.86	
NZ-05	-39.148381	175.610769	1954	56.86	

Same information as in Table 1. (??) indicates that the coordinates of the site or the reference field is not known or uncertain

3 Rock-magnetic analysis

Several rock-magnetic analyses were performed to identify the rock magnetic behaviour of the samples, to divide them into different rock magnetic groups (de Groot et al., 2015) and to improve the paleointensity experiments later on. To determine the magnetic carriers in the samples, the Curie temperature was identified using a horizontal translation type Curie balance (Mullender et al., 1993). Samples were placed in a field cycling between a B_{max} of 300mT and a B_{min} of 100mT, the magnetization was measured while heating to 620°C. Because the main aim of the experiment was to obtain as accurately as possible the Curie temperature(s) of the sample, the temperature was not lowered during the experiment to check for possible alteration. Curie temperatures were derived from the magnetization against temperature plot using the two-tangent method. The Curie temperatures of samples from the 16 different sites are shown in Table 3. None of the sites have a Curie temperature of pure magnetite (580°C). The sites from Iceland have the lowest Curie temperatures of <180°C. Several measurements on site IL-04 show it has varying Curie temperatures, with one sample resulting in a Curie temperature around 160°C and one sample with two Curie temperatures of 400/505°C. The sites from New-Zealand all show higher Curie temperatures between 280 and 507°C, NZ-20-5 has two Curie temperatures (examples shown in Figure 5).

The samples are grouped into rock-magnetic groups based on their Curie temperatures. Samples of Group L have low Curie temperatures between 100 and 200°C. All sites from Iceland are within this group, except that a second measurement on IL-04 results in two high Curie temperatures. Because the Curie temperature of the other samples from Iceland is low they are prone to viscous overprints. Samples of Group M either have various Curie temperatures or Curie temperatures higher than 200°C but below 500°C. All sites from New-Zealand are within this group, and possibly IL-04.

Table 3: Rock magnetic analyses results. Given are the Curie temperatures of the samples (T_c) and their rock magnetic group.

Iceland			New-Zealand		
Site	T_c (°C)	Group	Site	T_c (°C)	Group
IL-01	158	L	NZ-01	328	M
IL-02	158	L	NZ-02	470	M
IL-03	177	L	NZ-03	281	M
IL-04	160 or 400/505	L or M	NZ-04-1	414	M
IL-05	126	L	NZ-04-2	338	M
IL-06	129	L	NZ-04-3	353	M
IL-08	133	L	NZ-04-4	416	M
IL-09	170	L	NZ-05	300/507	M

Magnetic hysteresis was measured using a MicroSense vibrating sample magnetometer (VSM) to derive the saturation magnetization (M_s), remanent saturation magnetization (M_{rs}) and coercive force (B_c) from the hysteresis loop and the remanent coercive force (B_{cr}) from the back-field (or DCD) curve. The saturating field was set at 1.5T, the linear slope from 1T onwards was removed by automatically manipulating the data to remove the contribution of paramagnetic particles to the signal from the sample.
To determine the domain state of the samples, whether they are single domain (SD), pseudo-single domain (PSD), or multidomain (MD), the ratios of M_{rs}/M_s versus B_{cr}/B_c were plotted (Day et al., 1977). Single domain grains are M_{rs}/M_s >0.5; B_{cr}/B_c <1.5, PSD grains are M_{rs}/M_s between 0.05 and 0.5; B_{cr}/B_c between 1.5 and 4 and MD grains are M_{rs}/M_s <0.05; B_{cr}/B_c >4 (De Groot et al., 2014). All sites (Figure 6), except site IL-04, fall within the PSD range. Most sites fall on or close to the theoretical SD+MD mixing curves (Dunlop, 2002, Figure 6). Site IL-05, IL-09, NZ-01 and NZ-04-3 plot however further to the top right of the Day Plot which is closer to the

SP+SD mixing line. The mixing lines are created for pure magnetite samples, which is not the case for these samples, but nevertheless the location of these samples in the Day plot indicates a larger contribution of superparamagnetic particles.

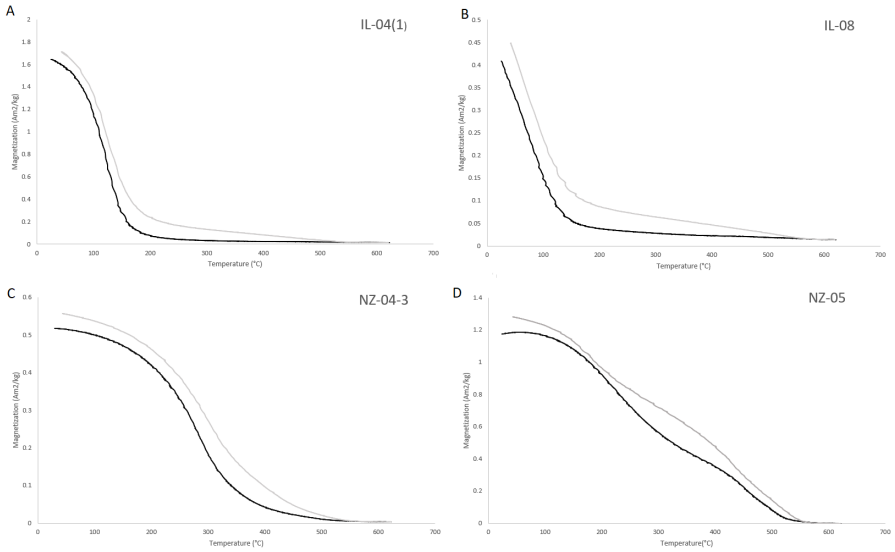

Figure 5: Examples of Curie measurement plots A) IL-04, sample 1 with a Curie temperature of 160° C, B) IL-08, T_c= 133° C, C) NZ-04-3, T_c= 353° C and D) NZ-05, two Curie temperatures of 300 and 507° C.

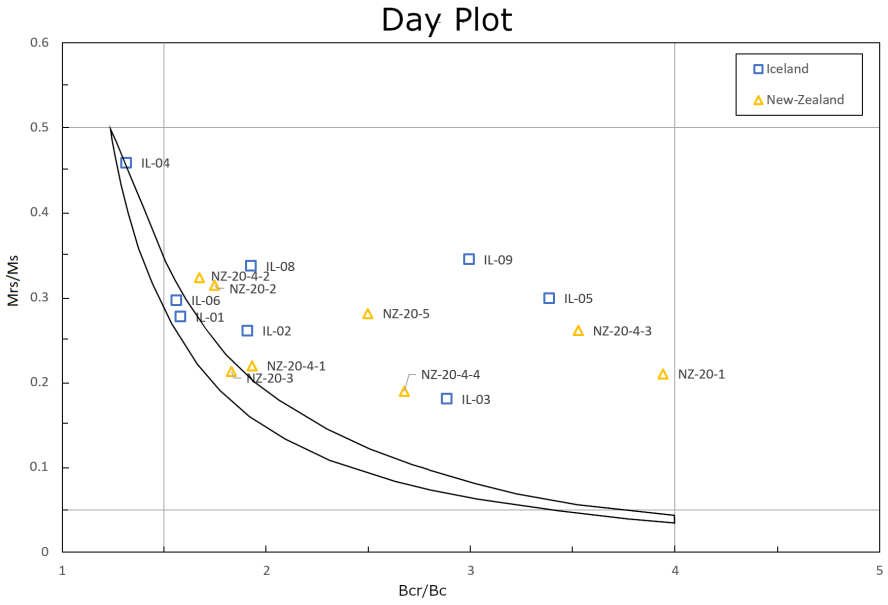

Figure 6: The Day Plot (Day et al., 1977) that indicates the domain state of the samples. Blue squares are the samples from Iceland, orange triangles the samples from New-Zealand. Except for IL-04, all sites fall within the pseudo-single domain range. Shown is the theoretical SD+MD mixing line (Dunlop, 2002)

4 IZZI-Thellier experiments

The IZZI-Thellier technique (Tauxe and Staudigel, 2004) is widely used for paleointensity research and is in this study applied to the samples from Iceland and New-Zealand for two main reasons. The first is to see how successful this technique is in calculating the paleointensity of these samples and to compare that later on with the other paleointensity techniques. The second is to check whether the flows from Iceland and New-Zealand indeed cooled in high-magnetic fields. For some sites, as shown in Table 1 & 2, the reference paleointensity is uncertain. Therefore, the results of the IZZI-Thellier technique in this study are compared with the reference paleointensity as calculated by the IGRF model (2019).

The IZZI-Thellier technique combines the ZI-method (Coe, 1967) and the IZ-method (Aitken et al., 1988), alternating between them so that at every other temperature step there is a change from "in-field/zero-field" to "zero-field/in-field". There is a pTRM check (Coe, 1967) after each IZ step. Prior to the IZZI-Thellier technique the directions of the samples were obtained from a robotized 2G DC-SQUID magnetometer with alternating fields (see next section pseudo-Thellier experiments). The directions were visualized in Zijderveld diagrams and analysed in paleomagnetism.org (Koymans et al., 2016). From the 16 sites, five sites were not used because their Zijderveld diagrams in paleomagnetism.org show large overprints which could lead to unsuccessful IZZI-Thellier measurements. The other 11 sites were chosen to be subjected to the IZZI-Thellier measurements. To make sure the samples did not outrange the 2G DC-SQUID magnetometer, the samples were small and glued into glass cups with quartz wool and kalium-silicate. First two samples of each site were thermally demagnetized to determine the temperature steps to use for the IZZI-Thellier technique. They were demagnetized in steps of 100, 170, 240, 310, 380, 450, 520 and 590°C. Eight samples per site were made for the IZZI-Thellier measurements. For batch 1, smaller and lower temperature steps of 100, 130, 160, 190, 220 and 250°C were chosen for the IZZI-Thellier measurements. Larger temperature steps of 240, 280, 320, 360, 410, 465 and 520°C were chosen for batch 2. For the in-field steps a DC field of 50μT was applied. The sites from Iceland were grouped to batch 1 and the sites from New-Zealand in batch 2. Site NZ-05 lost some of its magnetization at 300°C and some at 560°C, this site was divided over the two batches to see which one would give the best results.

The IZZI-Thellier dataset was interpreted in paleointensity.org (Béguin et al., 2020). The NRM remaining vs pTRM gained is shown in Arai diagrams (Nagata et al., 1963). The CCRIT and SELCRIT2 (with adding the criteria that k$\prime$ <0.164) selection criteria are applied to assess the quality of the results and the auto interpret function of paleointensity.org was used.

4.1 Iceland

Samples from Iceland generally lost all of their magnetization around 200-250°C, except for site IL-04 which was therefore subjected to additional higher temperature steps of 280 and 310°C. All five measured sites from Iceland (34 samples out of 40) passed the SELCRIT2 criteria. 4 sites (19 samples out of 40) passed the CCRIT criteria, which is a stricter set of selection criteria. Only site IL-03 did not pass the CCRIT selection criteria, mostly due an upward curvature in the Arai plot (Figure 7).
See for all results Table 4. The reference paleointensity from Iceland is 51.6 or 51.9μT (IGRF-13, 2019), depending on the age of the flows. To compare the measured paleointensity with the reference paleointensity, the intensity error fraction (IEF) (Biggin et al., 2007) was calculated.

$$IEF = \frac{I_{Meas} - I_{Ref}}{I_{Ref}} \; x \; 100$$

The IEF from site IL-03 is +18.99, meaning the IZZI-Thellier result largely overestimates the known paleofield. All other IZZI-Thellier results slightly underestimate the field. However, the IEF for these sites is still smaller than 10 and the reference paleointensity is within the standard

deviation (σ). Therefore, we assume the paleointensity of the Iceland flows is indeed high around 50μT and site IL-02, of which the coordinates were next to the flows' location, is indeed from a 1980 flow.

4.2 New-Zealand

All six measured sites of New-Zealand (35 samples out of 48) passed the SELCRIT2 criteria and 3 sites (10 samples out of 48) passed the CCRIT criteria. Most Arai plots, including those from Iceland, have pTRM-checks at their original datapoints which indicates there is no to minor chemical alteration (Figure 7). There are two sites for which the paleointensity is certainly known: NZ-04-3 and NZ-05. NZ-04-3 overestimates the field slightly and NZ-05 has a large negative IEF and underestimates the field. The paleointensity of NZ-02 should be around 56μT as well. NZ-02 is from a 1954 flow according to the sample summary, but its locations implies that is is an 1870 flow according to the map in Figure 4. But because the IZZI-Thellier result is low, an IEF of -20.28 (SELCRIT2) and -21.42 (CCRIT), this has to be considered carefully in the pseudo-Thellier and EMMA outcomes. Furthermore, for these three sites the IEF is larger for the CCRIT criteria than for the SELCRIT2 criteria even though the former is a stricter selection criteria. The other three sites for which the age is unknown and therefore also the paleointensity: NZ-01, NZ-04-1 and NZ-04-2, give high measured paleointensities between 51-61μT. Which would confirm a high paleofield.

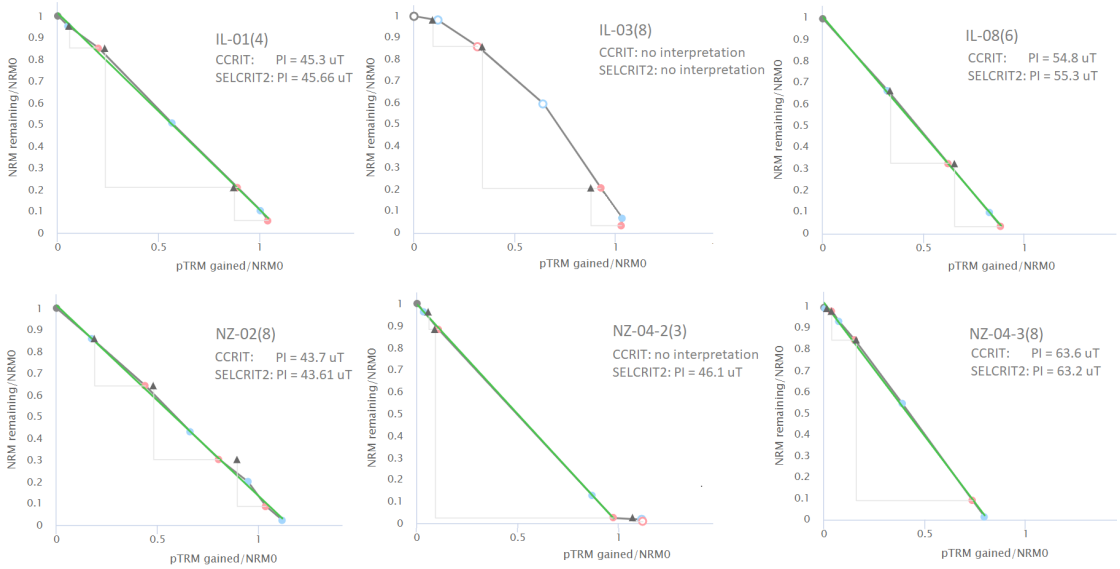

Figure 7: Examples of Arai plots from the IZZI-Thellier experiments of six sites, three specimens from Iceland and three from New-Zealand. Given are the corresponding paleointensity results for the CCRIT and SELCRIT2 selection criteria. Blue dots are the ZI steps, red dots are the IZ steps and black triangles are the pTRM checks. The green line is the largest interpreted segment. Some samples, such as NZ-04-2(3), lost almost all magnetization between two temperature steps and did not pass CCRIT.

Table 4: IZZI-Thellier experiment results

			SELCRIT2						CCRIT					
Site	Age	Href (μT)	n/N	#int	Hx (μT)	σ (μT)	σ/ Hx	IEF	n/N	#int	Hx (μT)	σ (μT)	σ/ Hx	IEF
Iceland														
IL-01	1970	51.63	6/8	47	49.27	4.74	9.6%	-4.57	4/8	15	48.50	3.70	7.6%	-6.06
IL-02	1980	51.92	8/8	44	50.21	3.62	7.2%	-3.29	4/8	8	47.51	3.55	7.5%	-8.49
IL-03	1981	51.92	5/8	14	61.78	5.67	9.2%	18.99	-	-	-	-	-	
IL-04	1981	51.92	7/8	81	49.00	5.68	11.6%	-5.62	4/8	20	47.67	4.37	9.2%	8.19
IL-08	1980	51.92	8/8	25	49.80	3.17	6.4%	-4.08	7/8	16	50.01	2.91	5.8%	-3.68
New-Zealand														
NZ-01	Post 1.85ka	??	7/8	50	60.98	4.26	7.0%	-	2/8	3	60.00	2.71	4.5%	-
NZ-02	1954 (?)	56.86	6/8	36	45.33	2.21	4.9%	-20.28	3/8	14	44.68	1.31	2.9%	-21.42
NZ-04-1	Historic	??	5/8	24	52.52	3.62	6.9%	-	-	-	-	-	-	-
NZ-04-2	Historic	??	5/8	10	51.51	1.79	3.5%	-	-	-	-	-	-	-
NZ-04-3	1954	56.86	8/8	71	61.43	3.19	5.2%	8.04	5/8	19	62.39	1.91	3.1%	9.73
NZ-05	1954	56.86	4/8	23	48.14	1.42	2.9%	-15.34	-	-	-	-	-	-

Given per site are the age of the lavaflow, the reference IGRF field value (Href), amount of samples that passed the selection criteria (n), amount of samples measured(N), amount of interpretations (#int), measured average paleointensity (Hx), the standard deviation (σ), standard deviation divided by the measured paleointensity, and the intensity error fraction (IEF) for the SELCRIT2 and the CCRIT selection criteria.

5 Pseudo-Thellier experiments

Where during the IZZI-Thellier method the samples are heated, the pseudo-Thellier technique applies alternating fields at room temperature to remove and impart magnetizations. Three samples from each site, sliced in half, so a total of 96 samples, were subjected to pseudo-Thellier experiments. They were first demagnetized in a robotized 2G DC-SQUID magnetometer with stepwise increasing alternating fields of 0, 2.5, 5, 7.5, 10, 15, 20, 25, 30, 40, 50, 60, 70, 80, 100, 150, 225 and 270mT (step 1). With the same alternating fields and a DC bias field of 40μT the samples were given a partial anhysteretic remanent magnetization (step 2). The pARMs were demagnetized again with the same alternating fields (step 3), to compare the NRM-demagnetization slope to the ARM-demagnetization slope. This is normally done to check whether the criterium that the ARMs were carried by the same grains as that carried the NRM was fulfilled (De Groot et al., 2016).

In the next section, chapter 6, the pseudo-Thellier data is used in the End-Member Modelling Analysis Approach. But first, the pseudo-Thellier data is analysed using the classical calibrated pseudo-Thellier approach from De Groot et al. (2013) to compare the results of these paleointensity techniques. The pseudo-Thellier data was analysed with paleointensity.org and the results are assessed with the pTH-SCRIT selection criteria proposed by Béguin et al. (2020), with the auto-interpretation function of paleointensity.org. Additionally, the $B_{1/2ARM}$ selection criteria from De Groot et al. (2013) is applied and only samples with a $B_{1/2ARM}$ between 23 and 63mT are used. The obtained pseudo-Thellier slopes are converted into absolute paleointensity data using the calibration relation formula of De Groot et al., 2016: B_{abs}=7.718 x ‖pTh‖+14.6.

5.1 Iceland

Of the eight sites from Iceland who were subjected to the pseudo-Thellier experiments, four sites with a total of 17 samples passed the pTh-SCRIT selection criteria applied in paleointensity.org. Of these samples, 13 had a $B_{1/2ARM}$ between 23 and 63mT and are used for further interpretation. The other five had a $B_{1/2ARM}$ below 23mT, on average the $B_{1/2ARM}$ for all 48 samples from Iceland was only 24mT. The pseudo-Thellier results are shown in Table 5, all results including the discarded sites are in Supplementary Table 1. Only the mean pseudo-Thellier slope of site IL-08 gives a paleointensity close to the reference value, with an IEF of -0.93. This site was also the most successful since all six samples passed the selection criteria (Table 6). The pseudo-Thellier results of IL-04, IL-05 and IL-09 were less successful and the calculated paleointensity is far below their reference paleointensity, with IEFs of -23.54, -15.95 and -34.25, respectively.

5.2 New-Zealand

The samples from New-Zealand were somewhat different from Iceland because an orientation was provided. Therefore, they were carefully measured while keeping that orientation in mind. Samples were sliced in half so that for example NZ-3A and NZ-3B come from the same sample, as well as NZ-3C and NZ-3D and so on. The direction of the field was not of particular interest for this study, but the directions can be identified in paleomagnetism.org (Koymans et al., 2016).

Of the 48 samples from eight sites in New-Zealand that were subjected to the pseudo-Thellier experiments, 24 passed the pTh-SCRIT selection criteria. Six of these samples passed these selection criteria because they were interpreted between fields of 70-270mT, but they had unrealistically low pseudo-Thellier slopes (a slope <1, Supplementary Table 1). Therefore, they are excluded from further interpretation. All samples show a very high $B_{1/2ARM}$, the average of all 48 samples is 77mT, and of the remaining 18 samples only five have a $B_{1/2ARM}$ between 23 and 63mT, they are from site NZ-03, NZ-04-1 and NZ-04-2 (Table 5). Again, using the calibration relation the pseudo-Thellier results are converted to absolute paleointensities, which range from 29 to 34μT. For site NZ-03, the 1870 or 1954 flow, the reference paleointensity is known, and the difference is

very large with an IEF of -49.00. The pseudo-Thellier results of NZ-04-1 and NZ-04-2 are around 33μT which is 20μT lower than the IZZI-Thellier results.

Table 5: Pseudo-Thellier results of Iceland and New-Zealand

Site	Href	n/N	#int	pTh	σ	σ/pTh	Hx	IEF
Iceland								
IL-01	51.63	0/6	-	-	-	-	-	-
IL-02	51.92	0/6	-	-	-	-	-	-
IL-03	51.92	0/6	-	-	-	-	-	-
IL-04	51.92	2/6	6	3.25	1.04	32%	39.68	-23.54
IL-05	51.92	1/6	2	3.76	0.01	0.27%	43.62	-15.95
IL-06	51.92	0/6	-	-	-	-	-	-
IL-08	51.92	6/6	38	4.77	0.39	8.18%	51.41	-0.93
IL-09	52.00	4/6	14	2.53	0.53	20.95%	34.13	-34.25
New-Zealand								
NZ-01	??	0/6	-	-	-	-	-	-
NZ-02	56.86	0/6	-	-	-	-	-	-
NZ-03	56.86	2/6	20	1.87	0.38	20.32%	29.03	-48.94
NZ-04-1	??	1/6	13	2.68	0.06	2.24%	35.28	-
NZ-04-2	??	2/6	9	2.2	0.1	4.55%	31.58	-
NZ-04-3	56.86	0/6	-	-	-	-	-	-
NZ-04-4	56.86	0/6	-	-	-	-	-	-
NZ-05	56.86	0/6	-	-	-	-	-	-

Given per site are the expected paleointensities based on their age (Href), amount of samples that passed the selection criteria (n), the amount of samples measured (N), amount of interpretations (#int), the pseudo-Thellier slope as obtained from paleointensity.org (pTh), the standard deviation (σ), standard deviation divided by the pseudo-Thellier slope, the paleointensity the pTh-slope would give according to the linear pseudo-Thellier calibration relation (B_{abs}=7.718 x $\|pTh\|$+14.6; de Groot et al., 2016) (Hx), and the intensity error fraction (IEF)

Table 6: Accepted Pseudo-Thellier results of Iceland and New-Zealand

Site	Sample	Href	$B_{1/2ARM}$	pTh	Hx	#int	AF-segm.	IEF
Iceland								
IL-04	IL-4-C	51.92	30.7	2.79	36.13	5	15-100	-30.43
IL-04	IL-4-D	51.92	51.8	5.56	57.51	1	20-100	10.73
IL-05	IL-5-F	51.91	30.5	3.76	43.62	2	50-270	-16.02
IL-08	IL-8-A	51.92	32.2	4.41	48.64	9	20-270	-6.36
IL-08	IL-8-B	51.92	39.9	4.9	52.42	5	20-100	0.92
IL-08	IL-8-C	51.92	44.9	5.3	55.51	4	25-100	6.86
IL-08	IL-8-D	51.92	42.8	5.29	55.43	6	20-100	6.72
IL-08	IL-8-E	51.92	35.1	4.47	49.10	8	20-270	-5.47
IL-08	IL-8-F	51.92	35.4	4.47	49.10	6	20-100	-5.47
IL-09	IL-9-A	52.00	36.3	2.06	30.50	1	50-270	-41.28
IL-09	IL-9-B	52.00	32.9	3.61	42.46	1	50-270	-18.25
IL-09	IL-9-C	52.00	36.3	3.26	39.76	3	50-270	-23.45
IL-09	IL-9-F	52.00	44.9	2.21	31.66	9	30-270	-39.05
New Zealand								
NZ-03	NZ-3-A	56.86	35.1	3.01	37.83	2	50-270	-33.47
NZ-03	NZ-3-D	56.86	34.4	1.75	28.11	18	15-270	-50.57
NZ-04-1	NZ-4-C	??	62.2	2.68	35.28	12	0-70	-
NZ-04-2	NZ-5-A	??	60.3	2.28	32.20	4	0-80	-
NZ-04-2	NZ-5-F	??	61.2	2.08	30.65	3	0-80	-

Results per sample, similar data is given as in Table 6 but additionally the $B_{1/2ARM}$ (mT) and the range of AF-fields that are interpreted (AF-segm.) are given.

Table 6 shows the results for all samples. Even within site results there is a wide variety of paleointensity outcomes. For example samples from site IL-09 have pseudo-Thellier slopes which convert to paleointensities ranging from 30 to 42μT. The $B_{1/2ARM}$ is also very variable, 30mT for one sample from IL-04 and 51.8mT for the other sample. Furthermore, of the successful samples from New-Zealand the other half did not give a reliable result. For example, NZ-3-A gave a reliable result but the other half NZ-3-B did not.
The IEF for most samples is large and underestimates the field. When plotting the 18 accepted pseudo-Thellier results together with the calibration relationship of De Groot et al. (2016): B_{abs}=7.718 x ‖pTh‖+14.6 (Figure 8), it is clear most samples do not plot close to the linear line. The pseudo-Thellier slope as obtained from the measurements is lower than predicted from the calibration relation. Only seven samples, from the sites IL-04 and IL-08 from Iceland, have a pTh-slope higher than 4 and are in agreement with the calibration relation.

The results listed above show that the classical calibrated pseudo-Thellier technique calculates only a few paleointensities close to the expected value. The technique is unpredictable in calculating paleointensities for the samples from Iceland and New-Zealand. To hopefully improve the results, the End-Member Modelling Analysis is applied to the pseudo-Thellier data in the next section.

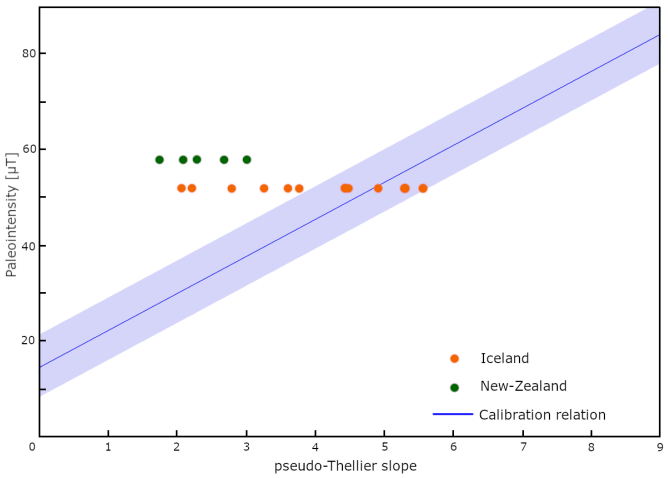

Figure 8: The calibration relationship of De Groot et al. (2016): B_{abs}=7.718 x ||pTh||+14.6. The green and orange dots are the accepted results with their expected paleointensity against the pseudo-Thellier slope. Seven samples from Iceland fall within the calibration relation range. All other samples have far lower pseudo-Thellier slopes than would be expected according to the formula.

6 End-Member Modelling Analysis (EMMA)

The success rate of the calibrated pseudo-Thellier was very low, six sites passed the selection criteria but only 1 site had a small IEF. Many pseudo-Thellier results in this study can not be reliably used because the $B_{1/2ARM}$ of the samples is very low (Iceland) or high (New-Zealand). The recently proposed EMMA-model by Liz van Grinsven (GR) avoids making such grain size selections and gives promising results. However, the calibration dataset which the EMMA-model uses to calculate end-members and paleointensities lacks samples with high paleofields. Here we add the samples from Iceland and New-Zealand to the calibration dataset. The goal is to see what the end-members of the new calibration dataset are and whether, when the paleointensity is calculated again, the data gives accurate results. Below is first shortly explained how the model works and what the previous calibration dataset contained, then the model is applied to the new calibration dataset with Iceland and New-Zealand.

Previous calibration dataset

The EMMA-model uses, as the name implies, end-members to calculate paleointensities. It takes as an input the same NRM demagnetization and ARM acquisition data as obtained for the classical pseudo-Thellier approach, but the NRM and ARM data is unmixed into constituent end-members. For the model to be able to do this correctly, a calibration dataset is needed. There are two steps which the model performs so we can make such a calibration dataset. First, the end-members in the dataset need to be determined. From these end-members the model calculates in the second step the paleointensity. Both steps can be explained by the following two equations on which the model is based:

$$X = H_x \cdot A \cdot E_x$$

$$Y = H_y \cdot A \cdot E_y$$

X = NRM demagnetization dataset
Y = ARM acquisition dataset
H_x = natural field strength (in this study the reference paleointensity)
H_y = lab field strength ($40\mu T$)
A = contribution of each end-members in a sample
E_x = end-members NRM demagnetization dataset
E_y = end-members ARM acquisition dataset
From Guided Research, Liz van Grinsven

Step 1: determine the end-members (X, Y, $\mathbf{H}_x$ and $\mathbf{H}_y$ are known)
The first step in the model is to determine the end-members in the dataset. X and Y are the NRM demagnetization and ARM acquisition data, respectively. To determine the end-members of the calibration dataset, samples are used of which the reference field H_x is known. H_y is the lab field, which is always set to 40μT. Because X, Y, H_x and H_y are known, the EMMA-model unmixes the NRM and ARM data using the non-negative matrix factorization algorithm in alternating iterations (Heslop and Dillon, 2007) to determine A, E_x and E_y. The full description of the EMMA-model and the mathematics behind it can be found in the Guided Research of Liz van Grinsven.

Step 2: calculate the paleointensity $\mathbf{H}_x$ (X, Y, $\mathbf{H}_y$, $\mathbf{E}_x$ and $\mathbf{E}_y$ are known)
The second step is to calculate the paleointensity from the calculated end-members. For the calibration dataset this is done as a check to see how accurately the model calculates the paleointensity. In the previous step, E_x and E_y were calculated, X and Y are still the same NRM and ARM data and H_y is the 40μT lab field. The model calculates the contribution of each end-member A again and the absolute paleointensity H_x of each sample. Because the reference paleointensity of the samples in the calibration dataset is known, EMMA also calculates the average (absolute) difference between the reference paleointensity and the paleointensity calculated by the model (Hx_{av} and Hx_{abs}). The model will calculate this for a large amount of iterations, step 1 and step 2 are continuously repeated, and the most accurate result is based on the iteration when the difference in paleointensity is the smallest (example: first column Figure 17). Ultimately, the goal of the EMMA-technique is to have a large calibration dataset and only apply this second step to samples of which the reference field is unknown, because the end-members E_x and E_y are then assumed to be universally determined.

These two steps have been performed before, on a dataset which consisted of 474 samples from Hawaii, Iceland, Tenerife, Reunion and Etna. When adding all NRM and ARM data from these samples to the model, the difference in reference and calculated paleointensity is quite large because not all samples work equally well. There are four options to modify the calibration dataset, to change which end-members are determined in step 1 and thereby improve the calculated paleointensity in step 2. These options are:

1. The amount of end-members into which the NRM demagnetization and ARM acquisition curves are unmixed needs to be chosen. The original dataset was most successful with a 3 end-member model, because a smaller or larger amount of end-members did not give more accurate results, i.e. a lower difference between reference and calculated paleointensity.

2. The second option is to remove outliers. The NRM demagnetization data is normalized by the maximum value of the ARM aquisition data for a sample and therefore most samples plot within a certain range. It is more difficult for the model to find communal end-members for samples that are far outside that specific range, those are the outliers. For the original dataset, 90% of the data was within a normalized NRMmax value of 0.7 to 3.9, samples outside this range are removed.

3. The third option is that it is possible to remove samples that have overprints. For this, the NRM demagnetization data is analysed using Zijderveld diagrams in paleomagnetism.org (Koymans et al., 2016) to check for possible overprints in the lower field steps. Each sample is given an alternating field step at which overprints are gone. The original dataset was most successful and still had a large amount of samples when only samples with overprints up to field step 2.5mT were in the dataset.

4. The last option is to remove unsuccessful locations. Data from Etna, Iceland and Tenerife gave rather poor results in the original dataset and thus a high difference between calculated and reference paleointensity, these locations were removed.

After each correction, the model performs step 1 and step 2 again for a certain amount of iterations. For the most optimal iteration it gives per sample the contribution of the different end-members (A), the paleointensity (Hx), the average difference between the calculated and reference paleointensity (Hx_{av}) and the absolute difference in paleointensity (Hx_{abs}). The most accurate previous dataset contained 167 samples and had a Hx_{av} of 0.0168μT and a Hx_{abs} of 5.8 μT.

New calibration dataset

To make a new calibration dataset, including samples with high paleointensities, the NRM demagnetization and ARM acquisition data from the 48 samples from Iceland and 48 samples from New-Zealand are added to the previous full dataset. The new dataset consist of Iceland*(old data), Reunion, Tenerife, Hawaii, Etna, Iceland(this study) and New-Zealand and contains 570 samples. The alternating field steps for Iceland and New-Zealand were 0, 2.5, 5, 7.5, 10, 15, 20, 25, 30, 40, 50, 60, 70, 80, 100, 150, 225 and 270mT. For the previous dataset these steps were similar, except for the last step which was 300mT instead of 270mT. The assumption was made that the decrease or increase in NRM and ARM data was linear between 225-300mT to calculate the magnetization at 270mT. All four modification steps explained above are repeated for the new dataset to find the most successful new calibration dataset. The amount of iterations was set to 1000. Checked after each calculation is whether the results of the model stabilize within 1000 iterations.

1. Amount of end-members

First the amount of end-members for which the model is most accurate needs to be determined. Hx_{av} and Hx_{abs} are calculated for models with 2 to 8 end-members, of which the results are shown in Figure 9. The model with 2 end-members has a low average difference in paleointensity (Hx_{av}, blue line) but a high absolute difference in paleointensity (Hx_{abs}, orange line). The results are most accurate when the amount of end-members is set to 3 (Hx_{av}=-2.08μT and Hx_{abs}=11.926μT) or 4 (Hx_{av}=-2.448μT and Hx_{abs}=11.949μT). The accuracy decreases for higher amounts of end-members. The 4 end-member model has approximately the same three end-members as the 3 end-member model (Figure 10) but between the orange and green line of the 3 end-member model, there is an additional end-member. So the third end-member in the 3 end-member model is approximately the fourth end-member in the 4 end-member model. Another observation is that the ARM acquisition curves of the 3 end-member model flatten quickly (Figure 10A). While in the 4 end-member model, after the initial steep increase, there remains a slight increase in the ARM acquisition curves (Figure 10B).

Samples from each location have their own distribution between these different end-members, which is A in the equations (Figure 11). Samples from Iceland have approximately equal contributions of each end-member. Reunion, Hawaii and Etna are mostly represented by end-member 1 and Tenerife consist for an even larger part of end-member 1. New-Zealand stands out because these samples consist almost entirely of end-member 3 (or 4 depending on the amount of end-members). Furthermore, the graphs of Iceland* and Iceland are very alike which should be the case since the samples come from the same blocks. Because the 3 and 4 end-member model give similar results the model is tested for the next three options: removing outliers, overprints and

locations for both amount of end-members. After applying these three options checked is which amount of end-members is most accurate. For the most accurate model of this new dataset the contribution of the different end-members for each location as in Figure 11 is calculated again.

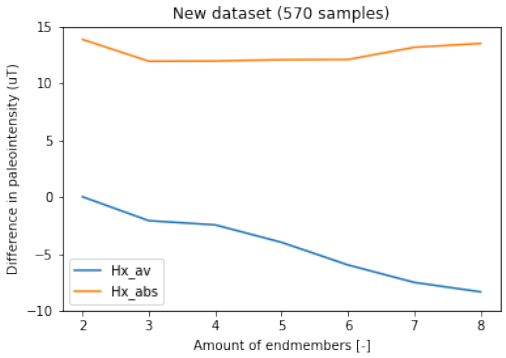

Figure 9: EMMA results for the full dataset with 570 samples, for the amounts of end-members 2 to 8. The blue line is the average difference between the calculated and reference paleointensity (Hx_{av}) and the orange line is the absolute difference in paleointensity (Hx_{abs}). Results for the 3 and 4 end-member model are most accurate.

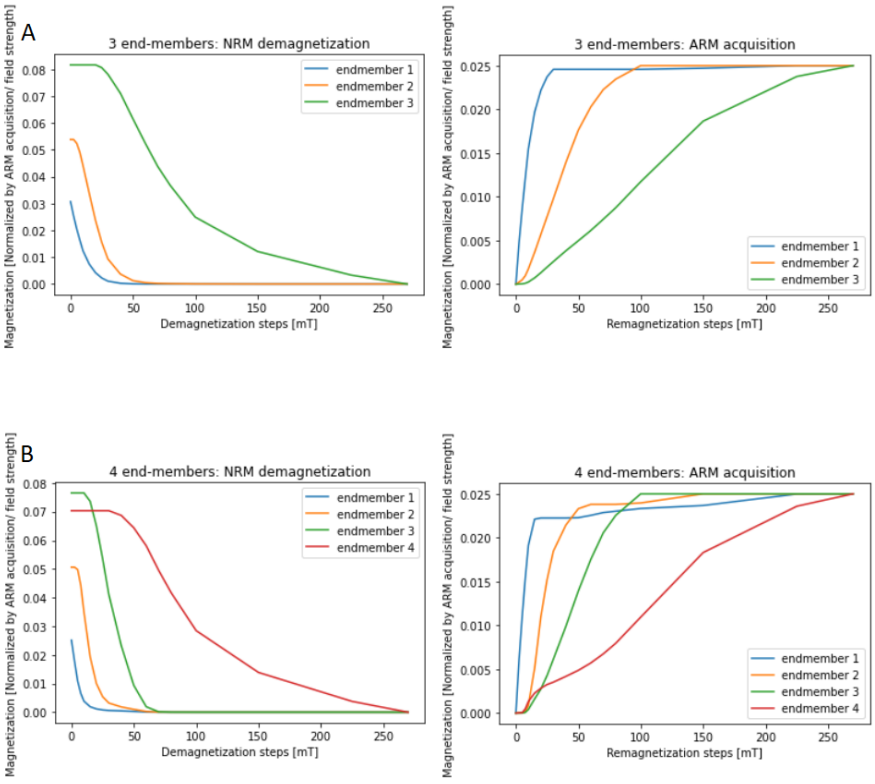

Figure 10: NRM demagnetization and ARM acquisition dataset. A) the end-members used for the entire dataset with a 3 end-member model, B) the end-members used with a 4 end-member model. End-member 3 in (A) is approximately end-member 4 in (B). The ARM acquisition curve in B does not flatten immediately.

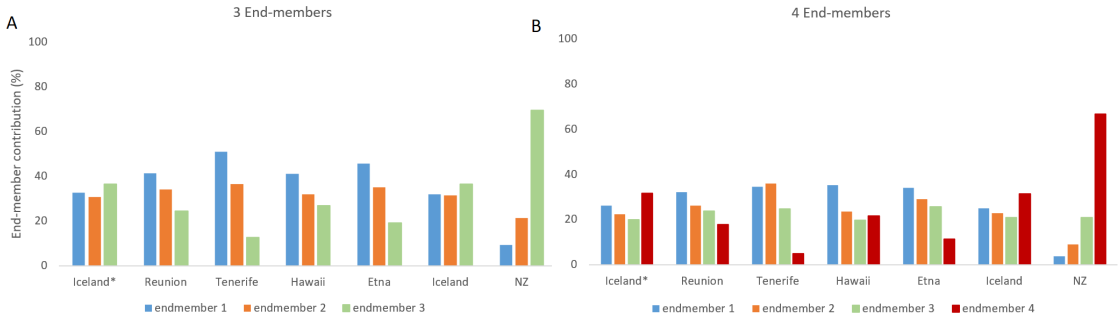

Figure 11: Contribution of the different end-members for each location for the full dataset with 570 samples without modifications for A) 3 end-member model and B) 4 end-member model.

2. Removing outliers

The second option is that it is possible to remove outliers. Figure 12 shows the distribution of the NRM demagnetization data of the new dataset normalized by the maximum value of the ARM acquisition data. Most samples plot between values of 0.8 and 4.0 (further on named NRMmax values), which are 515 samples and therefore 90% of the data. When the other 55 samples are removed, the 3 end-member model improves slightly to Hx_{av}=-1.828μT and Hx_{abs}=10.757μT. The 4 end-member model results in Hx_{av}=-2.336μT and Hx_{abs}=10.721μT.

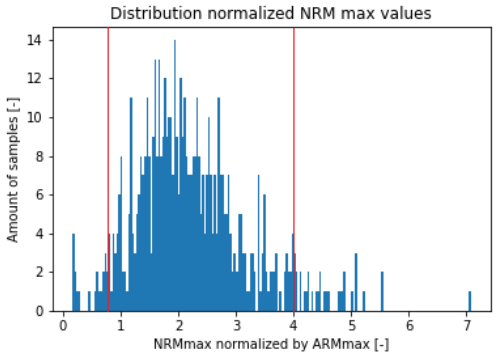

Figure 12: Distribution of the normalized NRM max values. 90% of the data is within values of 0.8 and 4.0 (red lines).

3. Removing overprints

The third option is to remove samples with overprints, which first needed to be identified. The NRM acquisition data of Iceland and New-Zealand was analysed in paleomagnetism.org to check for possible overprints in low-field steps. Especially samples from Iceland showed overprints in the lower field steps (Figure 13a+b), only five samples did not have an overprint at 2.5 or 5 mT. Of the samples from New-Zealand, site NZ-03 showed an overall non-linear trend towards the origin of the Zijderveld diagram (Figure 13d) and site NZ-04-4 often had overprints up to 7.5mT. Most other sites from New-Zealand did not show overprints after 2.5 mT (Figure 13c).

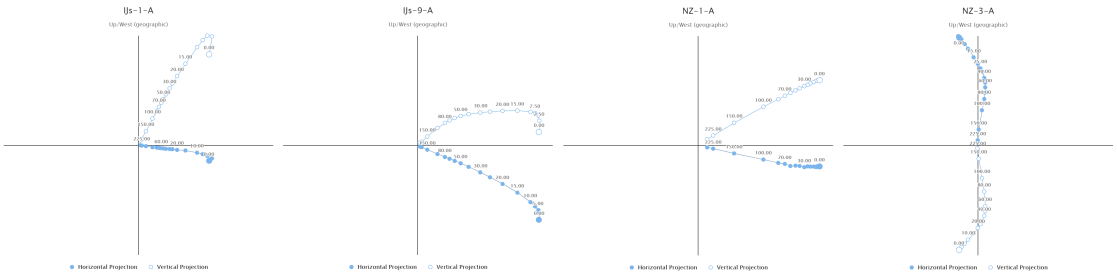

Figure 13: Zijderveld diagrams of two samples from Iceland and two from New-Zealand. All sites from Iceland show overprints in the low field steps. Some samples, such as IL-9-A and NZ-3-A, show an overall non-linear trend towards the origin of the Zijderveld diagram.

The EMMA model was run for the dataset without the outliers (those outside the 0.8 to 4.0 range of the NRMmax values) with 3 and 4 end-members, removing the samples that contain an overprint from different demagnetization field steps onwards. When the samples with an overprint are removed from fieldstep 0 mT, it means all samples with an overprint are removed. Removing the samples with an overprint from fieldstep 2.5 mT leaves samples in the model which have no overprint or only an overprint between 0-2.5mT. The results are plotted in Figure 14. When the samples with overprints from 0mT are removed the calculated absolute paleointensity, the continuous line, is closest to the reference paleointensity (Hx_{av}= -1.359μT : Hx_{abs}=7.482μT for 3 end-members and Hx_{av}= -1.368μT : Hx_{abs}=6.672μT for 4 end-members). However, in this case only 65 samples remain in the model (Table 7). When the samples with an overprint after 2.5 mT are removed the calculated absolute paleointensity gets less accurate but the average paleointensity, the dashed line, gets more accurate than when samples are removed from 0mT (Hx_{av}= -0.6058μT : Hx_{abs}=10.1302μT for 3 end-members and Hx_{av}= -0.613μT : Hx_{abs}=9.113μT for 4 end-members) and there are still 324 samples in the model. When the samples with overprints from 5mT are removed the 4 end-member model stays approximately equally accurate but the 3 end-member model results decline. Therefore, for the next steps the samples with overprints after fieldstep 2.5mT are removed. The 4 end-member model (orange line) has a slightly smaller difference between calculated and reference paleointensity than the 3 end-member model (blue line).

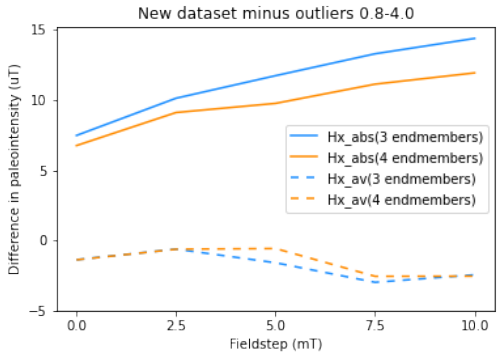

Figure 14: Dataset without outliers, removing the overprints from different field steps for the 3 and 4 end-member model. Continuous lines are the absolute difference in paleointensity, striped lines are the average difference in paleointensity for 3 end-members (blue) and 4 end-members (orange).

Table 7: Removing samples with overprints, for the dataset without outliers

		3 end-members		4 end-members	
Overprint removed	# samples	Hx_{av}	Hx_{abs}	Hx_{av}	Hx_{abs}
0mT	65	-1.359	7.482	-1.368	6.762
2.5mT	324	-0.606	10.130	-0.613	9.113
5mT	393	-1.577	11.734	-0.564	9.764
7.5mT	431	-2.967	13.293	-2.541	11.132
10mT	464	-2.432	14.385	-2.531	11.933

From which fieldstep samples with overprints are removed, the amount of samples that are still in dataset and the Hx_{abs} and Hx_{av} results for the 3 and 4 end-member model

4. Removing unsuccessful locations

The last option is to remove unsuccessful locations. To determine whether there are locations that on average give less accurate results than others, Hx_{av} and Hx_{abs} are calculated separately for each location with a 3 and 4 end-member model (Table 8), minus outliers and overprints from 2.5mT.

Table 8: Emma-modelling results for each location minus outliers 0.8-4.0 and overprints from 2.5mT

			3 End-member model			4 End-member model		
Location	n/N	Href	Hx	Hx_{av}	Hx_{abs}	Hx	Hx_{av}	Hx_{abs}
Iceland*	41/92	51.85	47.15	-4.70	12.84	47.28	-4.57	13.31
Reunion	27/93	36.63	39.70	3.07	8.24	39.83	3.20	9.61
Tenerife	5/35	32.48	42.21	9.73	9.73	39.16	6.68	6.68
Hawaii	137/190	37.31	42.32	5.01	7.77	41.56	4.25	5.99
Etna	84/96	43.47	36.90	-6.57	11.51	38.24	-5.23	9.55
Iceland	5/48	51.85	65.69	13.84	16.57	67.90	16.05	16.82
New-Zealand	25/48	56.85	42.67	-14.18	15.38	41.98	-14.87	16.86
Average				-0.6058	10.1302		-0.613	9.113

EMMA-results for the different locations. Given are the number of samples after removing the outliers and overprints (n), the total amount of samples (N), the reference paleointensity (Href), the average calculated paleointensity (Hx), the average difference in paleointensity (Hx_{av}), the absolute average difference in paleointensity (Hx_{abs}) for the 3 and 4 end-member model and the final average result.

From Table 8 it is clear that especially the locations from this study, Iceland and New-Zealand, give poor results. To not discard these locations yet and immediately remove high paleointensities from the dataset, first the model is tested when Iceland* and Etna are removed from the dataset. Both locations have a Hx_{abs} around or over 10μT in the 3 and 4 end-member model (Table 8) which shows they are not very accurate and these locations were also unsuccessful and removed from the previous dataset. Because there are 25 samples for New-Zealand, samples from this location are divided into their sites to check how accurately the separate sites are. Only five samples from Iceland remained, which were those without an overprint. Some sites from New-Zealand, such as NZ-01 and NZ-04-4, were removed previously by the model because their NRMmax values were higher than 4.0.

Without Etna and Iceland*, the results get more accurate (Table 9). Hx_{av}= 0.01μT, Hx_{abs}= 7.944μT for 3 end-members and Hx_{av}= -0.256μT, Hx_{abs}=6.998μT for 4 end-members. Sites NZ-04-1 and NZ-04-2 from New-Zealand give very low calculated paleointensities of 26μT and 22μT. These sites were also the sites of unknown age. Even though the IZZI-Thellier results give high measured paleointensities, which is why in the EMMA-model they were first given a reference paleointensity of 56.86μT as well, the sites do not give reliable results with the EMMA-model. Because for a correct calculation of the corresponding end-members of a sample the reference paleointensity can not be wrong, NZ-04-1 and NZ-04-2 are removed from the dataset, which leaves 189 samples.

Table 9: Emma-modelling results for each location minus outliers 0.8-4.0, overprints removed from 2.5mT and minus Iceland and Etna*

			3 End-member model			4 End-member model		
Location	n/N	Href	Hx	Hx_{av}	Hx_{abs}	Hx	Hx_{av}	Hx_{abs}
Reunion	27	36.63	36.87	0.24	7.42	37.82	1.19	7.65
Tenerife	5	32.48	35.10	2.62	2.62	35.79	3.31	3.31
Hawaii	137	37.31	39.29	1.98	6.66	38.94	1.63	4.97
Iceland	5	51.85	59.67	7.82	10.93	59.12	7.27	10.84
NZ-02	5	56.86	52.45	-4.41	4.41	52.57	-4.29	4.29
NZ-04-1	6	56.86	26.79	-30.07	30.07	26.18	-30.68	30.68
NZ-04-2	4	56.86	22.30	-34.56	34.56	22.64	-34.22	34.22
NZ-04-3	4	56.86	64.49	7.63	7.63	65.35	8.49	8.49
NZ-05	6	56.86	53.32	-3.54	3.85	48.00	-8.86	8.86
Average				0.010	7.944		-0.256	6.998

The EMMA-model for this final calibration dataset consisting of 189 samples calculates for 3 end-members a Hx_{av}=-0.056μT and Hx_{abs}=6.497μT and for 4 end-members a Hx_{av}=-1.41μT and Hx_{abs}=4.932μT. Some sites (Table 10) give more accurate results in the 4 end-member model than in the 3 end-member model and vice versa. Furthermore, each time poor locations are removed some locations will give better results, for example Hawaii and Tenerife in Table 10 give better results than in Table 9. While others got worse after removing some locations, for example NZ-02 and NZ-05 give less accurate results in Table 10 than in Table 9. Compared to the results from the original dataset, Hx_{av} is less accurate for both the 3 and 4 end-member model and Hx_{abs} is more accurate with the 4 end-member model.

Table 10: Most accurate calibration dataset. Emma-modelling results for each location minus outliers 0.8-4.0, overprints removed from 2.5mT and minus Iceland, Etna, NZ-04-1 and NZ-04-2.*

			3 End-member model			4 End-member model		
Location	n/N	Href	Hx	Hx_{av}	Hx_{abs}	Hx	Hx_{av}	Hx_{abs}
Reunion	27	36.63	35.62	-1.01	7.24	32.59	-4.04	5.31
Tenerife	5	32.48	34.40	1.92	2.00	30.68	-1.80	3.00
Hawaii	137	37.31	38.00	0.69	6.35	36.55	-0.76	4.29
Iceland	5	51.85	54.83	2.98	7.69	48.37	-3.48	12.17
NZ-02	5	56.86	47.19	-9.67	9.67	47.66	-9.20	9.20
NZ-04-3	4	56.86	55.98	-0.88	1.13	68.20	11.34	11.34
NZ-05	6	56.86	47.87	-8.99	8.99	51.38	-5.48	5.70
Average				-0.056	6.497		-1.41	4.932

Final EMMA calibration dataset check

After modifying the dataset by applying the four options, the best results are shown in Table 10. This is for a 3 and 4 end-member model, with outliers, overprints and unsuccessful locations removed at 1000 iterations. Here is checked whether this amount of end-members at 1000 iterations still gives the most accurate result.

Amount of iterations

For a correct calibration dataset the difference in paleointensity should stabilize within the amount of iterations chosen, and the NRM demagnetization and ARM acquisition error should be as small as possible and stable. To check whether the final calibration dataset as in Table 10 is indeed most accurate with a 3 or 4 end-member model at 1000 iterations, the NRM demagnetization and ARM acquisition error for 2 to 5 end-members (Figure 15) and their resulting Hx_{av} and Hx_{abs} are compared. The NRM and ARM error is a thick blue line in the plots, but actually switches up and down because for every other iteration the model is calculated for the NRM demagnetization data or the ARM acquistion data. Both errors are still the smallest for the 3 and 4 end-member model. The model with 5 end-members gives low error percentages as well, but the difference in paleointensity and Hx_{av} is higher (-2.775μT).

The plots of the 3 and 4 end-member model stabilize within the 1000 iterations and the optimal iteration for the final dataset was within those 1000 iterations (Figure 15). As a check, the amount of iterations for the 3 and 4 end-member model was set to 3000 (Figure 16). A new optimal iteration was found for the 3 end-member model at 2250, which changed the results to Hx_{av}=-0.6021μT and Hx_{abs}=5.912μT. This is still close to the original outcome, but within site and location differences were high. For example, Hx_{av} of Tenerife and Iceland went up to -12.54μT and -9.51μT, respectively. Furthermore, the graphs that compare the difference in paleointensity and NRM demagnetization and ARM acquistion error plots do appear worse and unstable than when the iterations are set to 1000. So, for the final dataset the amount of iterations is kept at 1000.

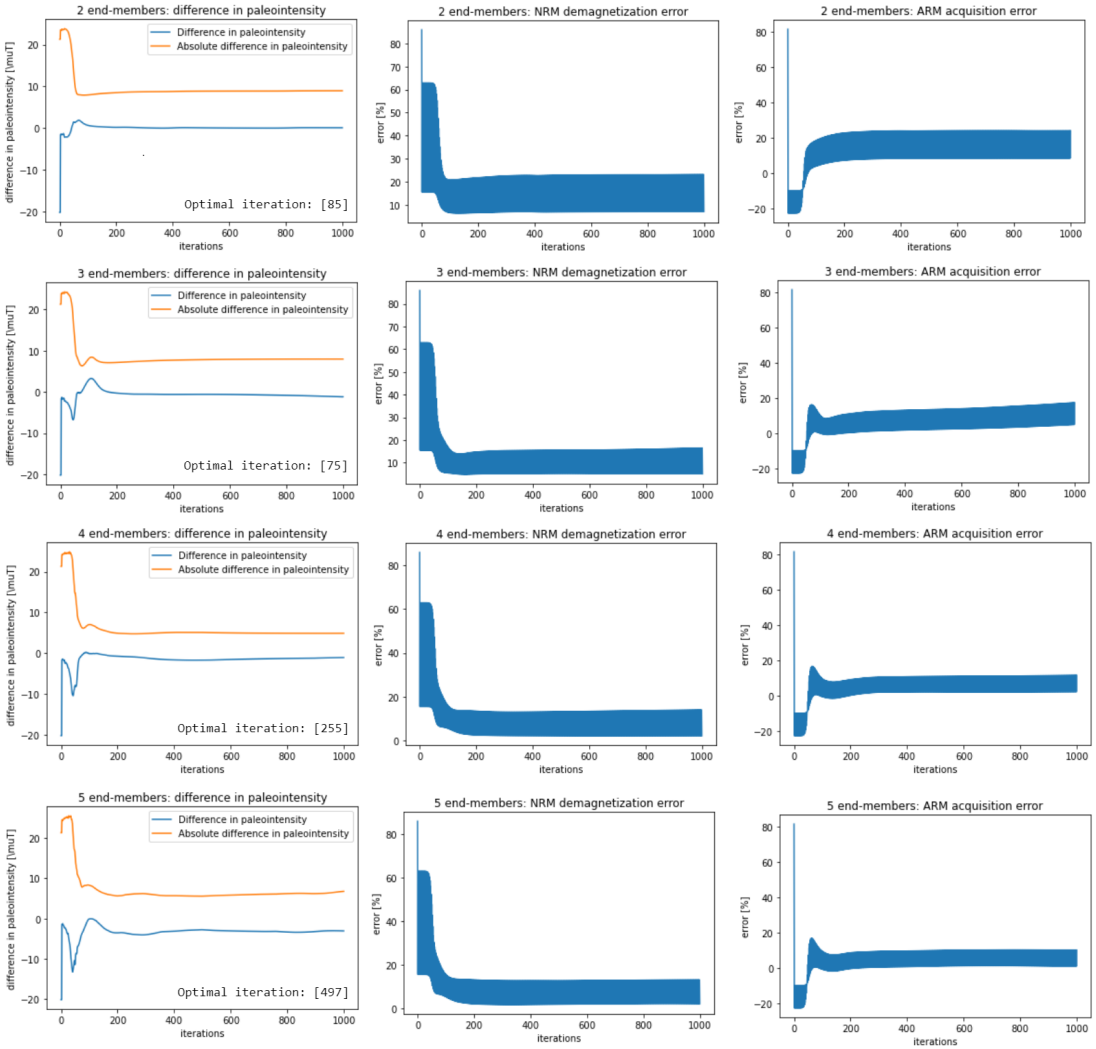

Figure 15: The optimal iteration over 1000 iterations for the dataset minus outliers, overprints from 2.5mT and Etna, Iceland, NZ-02, NZ-04-1 and NZ-04-2 for different amount of end-members. The first column shows the difference between Hx_{av} (blue line) and Hx_{abs} (yellow line), the second column the NRM demagnetization error over the 1000 iterations and the third column the ARM acquisition error for 1000 iterations.

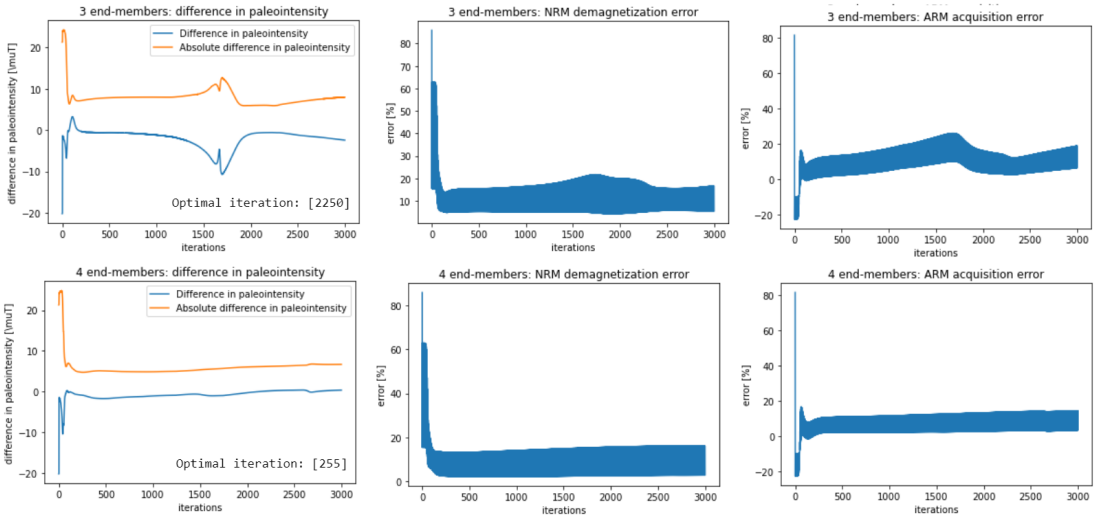

Figure 16: For 3 and 4 end-member model, the difference between Hx_{av} (blue line) and Hx_{abs} (yellow line), the NRM demagnetization error over 3000 iterations and the ARM acquisition error for 3000 iterations.

Final amount of end-members

Figure 15 already shows that the error percentages are lowest for the 3 and 4 end-member model. In Figure 17 the end-members which are calculated for the final dataset are shown for a 2, 3, 4 and 5 end-member model. For the model, it is preferred that the end-members used to calculate paleointensities are distinctly different. For a 5 end-member model, two end-members become very similar in the ARM acquisition end-member plots. End-member 2 and 3 are also very similar in the ARM acquisition plot of the 4 end-member model.

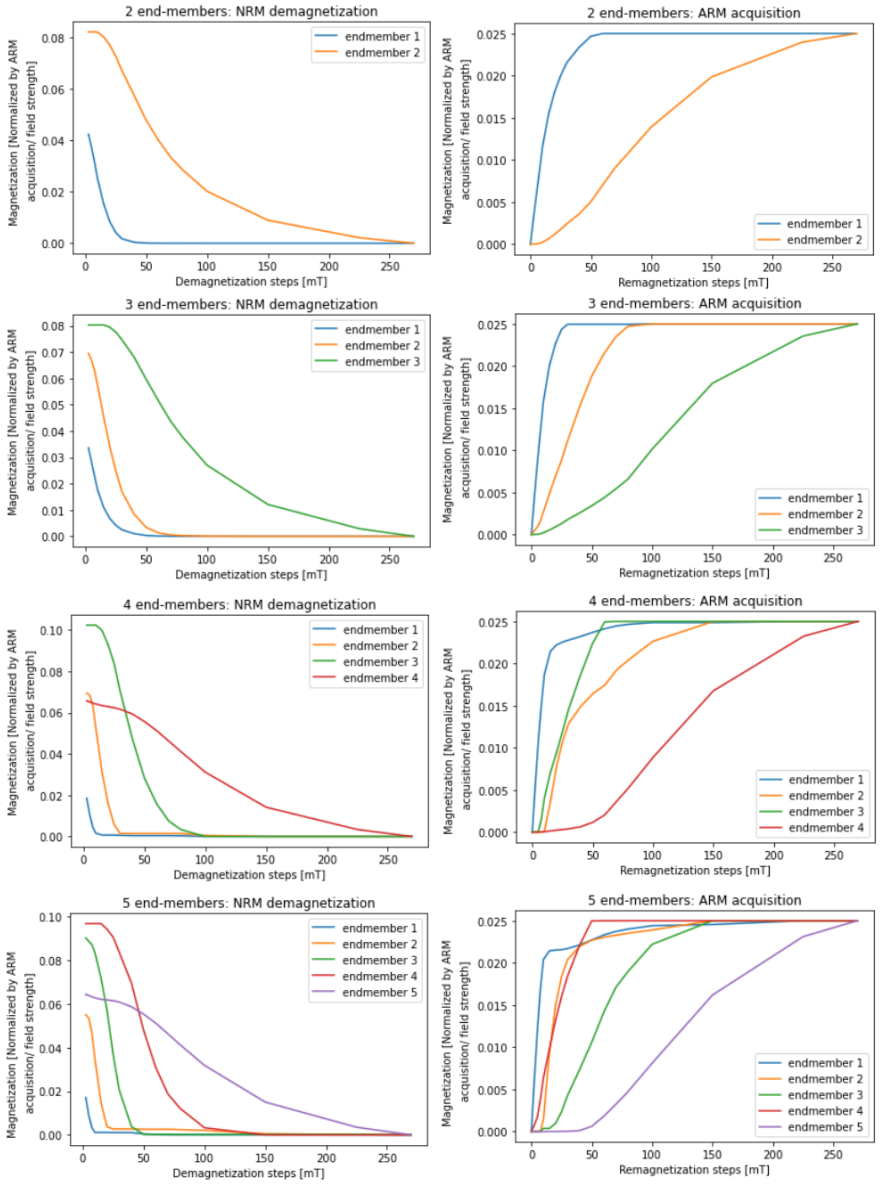

Figure 17: End-members calculated for the final dataset with a 2, 3, 4 and 5 end-member model. In the 4 end-member model, end-member 2 and 3 are similar. In the 5 end-member model, end-member 2 and 4 are similar.

The distribution of the end-members of the final dataset (Figure 18) shows that the contribution of the different end-members in the samples of Reunion, Hawaii and Iceland are still approximately equal. Tenerife consists mostly of end-member 1 or 2, and clearly lacks the presence of end-member 3/4. This last end-member is the dominant end-member for all three successful samples from New-Zealand. Samples from NZ-05 are even almost fully described by end-member 3 or 4.

The final results for the 3 or 4 end-member model were both approximately equally accurate, but because the 4 end-member model has two end-members which look similar in the ARM acquisition curves (Figure 17), the 3 end-member model has a lower average difference in paleointensity and none of the sites in the 3 end-member model have a Hx_{abs} higher than 10μT (Table 10), the 3 end-member model is preferred for the current calibration dataset. This results in a Hx_{av}= -0.056μT and Hx_{abs}= 6.497μT, which is slightly less accurate than the previous dataset without Iceland and New-Zealand.

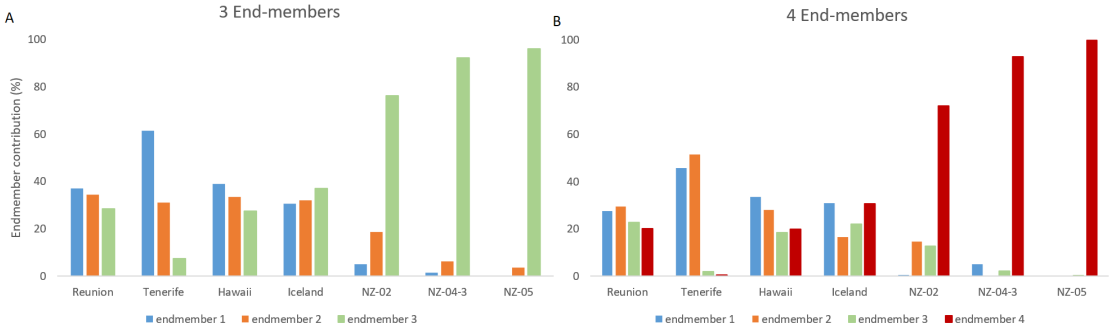

Figure 18: End-member distribution for the final dataset for the A) 3 and B) 4 end-member model

7 Discussion

The previous End-Member Modelling Analysis calibration dataset contained 167 samples, but lacked samples with high paleointensities. In this study, samples from Iceland and New-Zealand which cooled in natural fields >50μT were subjected to rock-magnetic analyses experiments and three different paleointensity techniques. Of the applied paleointensity techniques, the IZZI-Thellier technique was most successful, and the calibrated pseudo-Thellier technique the least. Some samples from Iceland and New-Zealand were successfully added to the EMMA calibration dataset. The EMMA-model gave the most accurate results for a model based on 3 end-members when outliers, overprints and unsuccessful locations were removed. The new EMMA calibration dataset gives accurate results for some sites and is able to calculate high paleointensities, but there are also some problems and remaining questions. In the next section the results from the EMMA-model are compared with rock-magnetic characteristics and the results from all three methods are discussed and compared with each other. Finally, some next steps to take to improve the EMMA-model are proposed.

End-members and rock-magnetic characteristics

The idea behind the EMMA-model was that each sample consists of different end-members with their own mapping between the acquired NRMs and ARMs. Figure 18 and 21 show that there is a lot of variety in the distribution of the percentage of each end-member per location. To test whether this is due to a different distribution of iron-oxides in the grains, which is reflected in the Curie temperatures of the samples, the end-member distribution of the separate flows from the locations of the final dataset are compared with their measured Curie temperatures. The Curie temperatures of Iceland and New-Zealand were determined in this study, Curie temperatures of Reunion are from Béguin (in prep) those of Tenerife are from de Groot et al. (2015) and those of Hawaii are from de Groot et al. (2012). When samples display more than one Curie temperature the dominant temperature is chosen. Sites with a gradual loss of Curie temperature (which are three from Hawaii) are left out. Figure 19A shows the Curie temperature against end-member contribution of the final most successful EMMA dataset. In this figure are four sites of Iceland, three sites of New-Zealand and one site of Tenerife. With increasing Curie temperatures, the contribution of end-member 1 and 2 decreases and the contribution of end-member 3 increases. The

samples with the highest Curie temperatures, which are those from New-Zealand, consist almost fully of end-member 3. With the addition of the samples from Hawaii (27 sites from 13 different dated flows) and Reunion (7 sites from 6 flows) the trend becomes less obvious (Figure 19B), but still the samples with a Curie temperature of 550°C have the largest contribution of end-member 3 and the contribution of end-member 1 is large for samples with a low Curie temperature. The sites in Figure 19 with their Curie temperature and end-member percentages can be found in Supplementary Table 2.

Such a link between Curie temperature and end-member contribution would confirm that the EMMA-model is accurate in determining different end-members which are based on rock-magnetic characteristics, and thus have a physical meaning. End-member 3 could in this case reflect magnetite, and end-member 1 and 2 have a larger contribution of titanium. The question remains why the samples from New-Zealand have such a distinctive end-member distribution and the samples from Hawaii, of which some have high Curie temperatures as well, have a less obvious distribution. A connection with grain sizes (from the Day plot) was not found, but it should be looked in whether the end-members are solely based on the titanomagnetite content (the mix between ulvöspinel and magnetite in the Ternary diagram Figure 2) or whether there are other factors or compositions that determine the end-members.

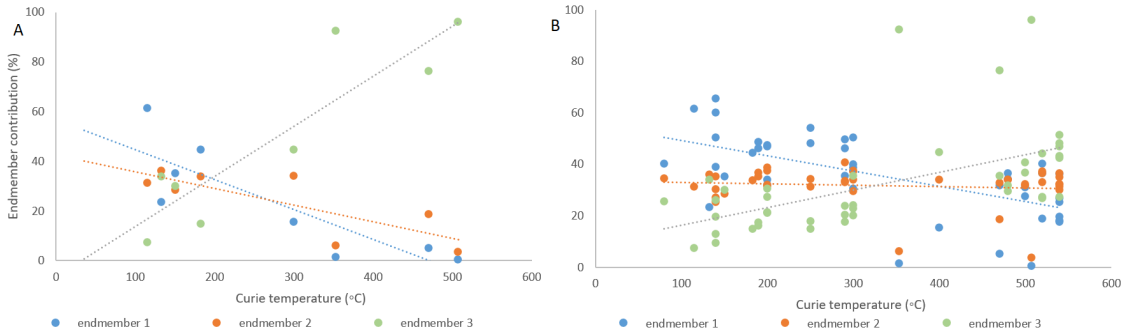

Figure 19: Curie temperature against end-member contribution of A) Iceland, New-Zealand and Tenerife and B) Iceland, New-Zealand, Tenerife, Hawaii and Reunion for a 3 end-member model of the dataset minus outliers, overprints from 2.5mT and Iceland and Etna.*

Comparing the paleointensity methods

The results for all three methods are shown in Table 11. The IZZI-Thellier method was surprisingly successful for the samples from Iceland and New-Zealand, with a success rate of 100% for the SELCRIT2 selection criteria and 64% for CCRIT selection criteria. This high success rate could be due to the careful sample preparation with small samples and/or the improved shielded room. Especially the sites from Iceland had measured paleointensities close to their reference value. The sites from New-Zealand were more problematic, also because for some sites the age was uncertain. NZ-04-1 and NZ-04-2 are of historic age, so no reference paleointensity is known, but IZZI-Thellier did give high paleointensities. With the EMMA-model, these sites gave very low paleointensities and were therefore removed from the final dataset. EMMA-3 and EMMA-4 give the results for the 3 and 4 end-member model, respectively. The EMMA-3 results compared to the IZZI-Thellier results give sometimes higher and sometimes lower paleointensities compared to the reference paleointensity, there does not seem to be a bias towards high or low paleointensities from one of the two methods.

Table 11: Results for all three methods

Sample	Href	IZZI-S	IZZI-C	p-TH	EMMA-3	EMMA-4
Iceland						
IL-01	51.6	49.27	48.50	-	52.51	45.26
IL-02	51.9	50.21	47.51	-	64.43	62.76
IL-03	51.9	61.78	-	-	-	-
IL-04	51.9	49.00	47.67	39.68	52.68	38.19
IL-05	51.9	x	x	43.62	-	-
IL-06	51.9	x	x	-	-	-
IL-08	51.9	49.80	50.01	51.41	40.09	32.87
IL-09	51.9	x	x	34.13	-	-
New-Zealand						
NZ-01	??	60.98	60.00	-	-	-
NZ-02	56.86	45.33	44.68	-	47.19	47.66
NZ-03	56.86	x	x	29.03	-	-
NZ-04-1	??	52.52	-	35.28	-	-
NZ-04-2	??	51.51	-	31.58	-	-
NZ-04-3	56.86	61.43	62.39	-	55.98	68.20
NZ-04-4	56.86	x	x	-	-	-
NZ-05	56.86	48.14	-	-	47.87	51.38

Given are the reference paleointensity (Href), the results from IZZI-Thellier SELCRIT 2 (IZZI-S), IZZI-Thellier CCRIT (IZZI-C), calibrated pseudo-Thellier (p-Th), 3 end-member model (EMMA-3) and the 4 end-member model (EMMA-4). An (x) means not measured, an (-) means no successful result.

The calibrated pseudo-Thellier technique was not very successful in this study, only site IL-08 passed the selection criteria and had a calculated paleointensity close to the reference paleointensity. All others did not pass the selection criteria or had low calculated paleointensities (Table 11 and Figure 8). The problem with various samples from Iceland was that their $B_{1/2ARM}$ was very low, and from those of New-Zealand the $B_{1/2ARM}$ was very high, therefore they were excluded from interpretation. Figure 20 shows the distribution of the successful samples and their $B_{1/2ARM}$ against the contribution of the different end-members. Samples with a high $B_{1/2ARM}$ have a larger contribution of end-member 3, they loose their magnetization in the higher alternating field steps which is in accordance with the slope of end-member 3 (Figure 17C). Similarly, the contribution of end-member 1 is largest for samples with a low $B_{1/2ARM}$. In the calibrated pseudo-Thellier approach, only the samples with a $B_{1/2ARM}$ between 23 and 63mT were selected. In the EMMA-model, the $B_{1/2ARM}$ of the successful sites range from 16.3 to 124.7mT, which is a much wider range.

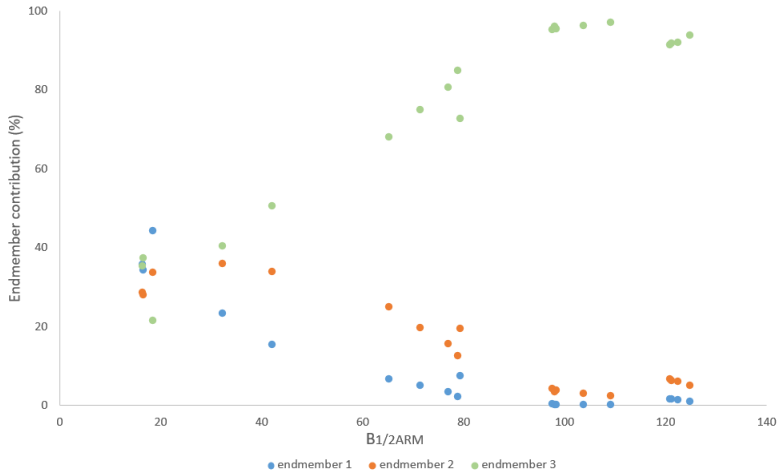

Figure 20: $B_{1/2ARM}$ (mT) against end-member contribution for the samples from Iceland and New-Zealand of the final dataset

Unsuccessful sites in the EMMA-model

With option 4 in the EMMA-model, locations and sites that gave inaccurate results were removed. Some locations were already removed from the model earlier due to for example a large degree of overprints, such as Iceland. For others it is unknown why exactly EMMA calculates paleointensities that are not comparable to their reference paleointensity or to results from the other techniques. For example, the IZZI-Thellier technique measured high paleointensities for NZ-04-1 and NZ-04-2, but with the EMMA model the calculated paleointensities were very low. It is interesting to note that these two sites, together with NZ-03 but that was already unsuccessful due to overprints, have a different contribution of end-members than the other sites from New-Zealand that were accurate (Figure 21). NZ-03, NZ-04-1 and NZ-04-2 have a contribution of all three end-members while the others are dominated by end-member 3. After NZ-04-1 and NZ-04-2 are removed from the dataset the paleointensity which the EMMA-model calculates decreases for all locations (Table 9). This also makes the result for NZ-02 and NZ-05 worse. A possible explanation for this is that even though the two samples have a smaller percentage of end-member 3 than the other samples from New-Zealand, it is still a lot more than the samples from Iceland, Reunion, Hawaii and Tenerife, but the exact reason is unknown. The paleointensity of New-Zealand seems to be described best by end-member 3.

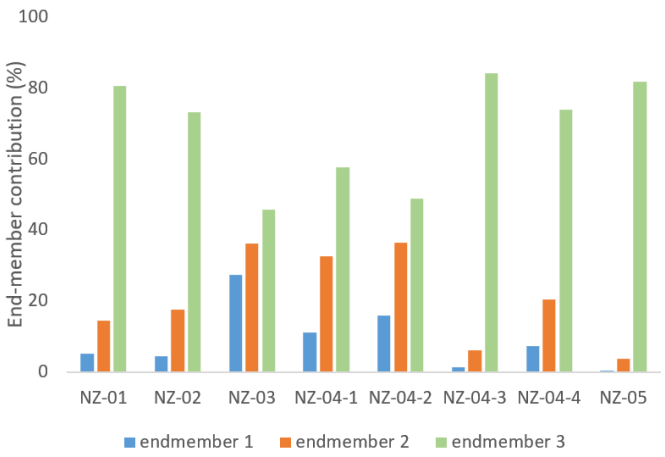

Figure 21: Distribution of end-members for sites of New-Zealand, for the original dataset with 570 samples. NZ-03, NZ-04-1 and NZ-04-2 have the smallest contribution of end-member 3 and their calculated paleointensities were very low.

For the final dataset the same behaviour is seen in the samples from Reunion. EMMA calculates for two sites from Reunion, of flow 1977 (with six samples) and flow 1986 (one sample), paleointensities higher than 10μT compared to their reference paleointensity. The flows from Reunion which are within a 10μT range from their reference paleointensity have the highest percentage of end-member 1, the 1977 and 1986 flow have the highest contribution of end-member 3 (Figure 22A). These observations suggest that the best results are found for locations with homogeneous lavaflows and a homogeneous distribution of end-members that will describe their reference paleointensity best. However, this is not seen in the sites from Hawaii. Sites from Hawaii with a difference in paleointensity more than 10μT are 1859 (three samples), 1990b (two samples), 1935b (four samples), 1919b (five samples) and 1859b (four samples) (Figure 22B). These sites do not have a particularly different distribution of end-members than the other sites from Hawaii. It must be noted that all sites from Reunion, Tenerife, Hawaii, Iceland and New-Zealand on average contain only four samples.

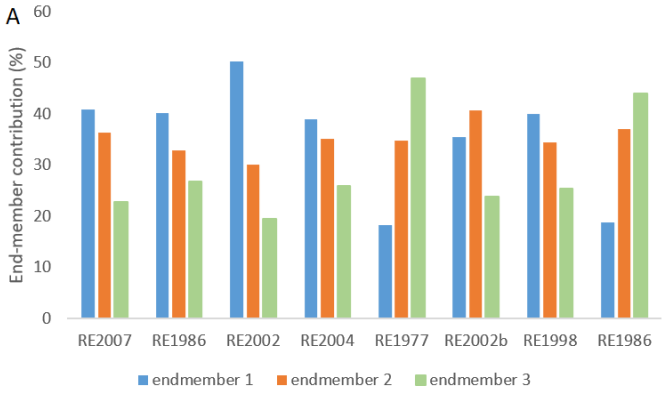

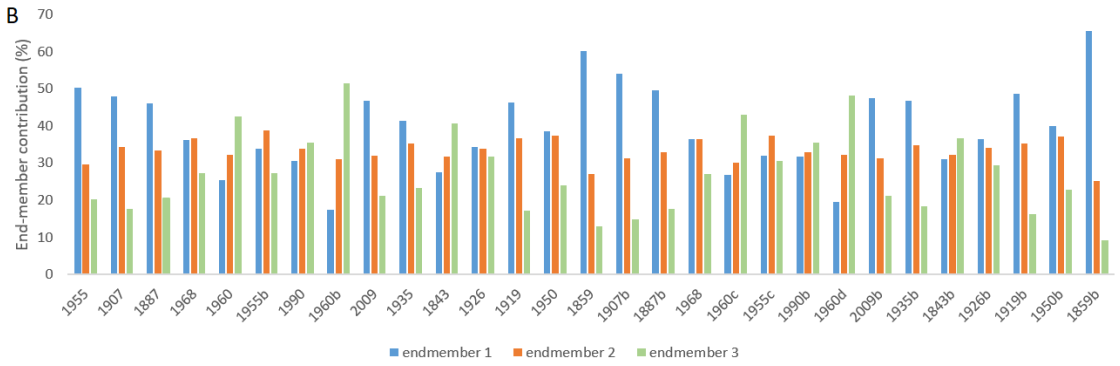

Figure 22: A) end-member distribution of the flows from Reunion for the final dataset. RE1977 and RE1986 gave inaccurate results with a paleointensity 10μT higher than expected. B) end-member distribution of the flows from Hawaii for the final dataset, 1859, 1990b, 1935b, 1919b and 1859b were unsuccessful.

Next steps

For a reliable End-Member Modelling Approach, it is crucial that the dataset to calculate the end-members is expanded, and there are several reasons for this. First, the updated end-member calibration dataset consists at the moment of 189 samples, of which 20 samples are from regions which high paleointensities (>50μT). The other 169 samples have reference paleointensities between 32.48 and 37.31μT. This is still a small range and a small dataset. The model is on average able to calculate high paleointensities for the samples from Iceland and New-Zealand, but possibly these results improve when more samples with high paleointensities are added to the dataset. Because there are no samples with low paleointensities in the dataset, it is unknown whether the model can accurate calculate such fields. Regions, and recent lavaflows, with low magnetic fields can be found in Central Andes which would add intensities of around 23μT to the dataset.

Second, 72% of the current dataset is represented by samples from Hawaii. These do not only have similar paleointensities but might also behave similarly if the grain compositions do not vary a lot. It is interesting to add more samples with very distinct end-members and with very low or high Curie temperatures to observe whether the connection with end-members is applicable to all samples. Samples with none to a minor amount of overprints are preferred because they seem to give the most accurate results.

Third, an expanded dataset might enlarge the amount of samples within a certain normalized NRM demagnetization range. For the current dataset, a range of 0.8 to 4.0 was selected because 90% of the current data was within that range. 13 of the 48 samples from New-Zealand had a normalized NRMmax value higher than 4.0 and were removed from the model. With a larger dataset this range will most likely increase.

Lastly, the ultimate goal of the EMMA-approach is to apply it to samples for which the paleointensity is not known. However, unsuccessful locations can be removed from the current dataset because the reference paleointensity is known. A criteria to select the sites which give accurate results, and to remove sites with inaccurate results, was not entirely found. Bad measurements in the results of Reunion and New-Zealand were found for sites with a different distribution of end-members compared to mean result of the other sites, but this relation is not seen in sites from Hawaii. After removing outliers, overprints and locations, on average there remain only four samples per site. To be able to identify bad measurements or entirely bad resulting sites, more samples per flow are needed. Hawaii had the largest amount of samples, and was also the most successful. It might be that with a larger amount of samples we find a check parameter, but also

that the result for a specific location improves altogether.

Finally, the paleointensity that each end-member represents in a sample individually has to be calculated to check whether there are large differences, and that the model does not just average the outcome.

8 Conclusion

Three different paleointensity methods applied to lavas from Iceland and New-Zealand, which cooled in very high natural magnetic fields (>50μT), were not equally successful. The IZZI-Thellier method was very successful, with a 100% and 64% success rate for the SELCRIT2 and CCRIT selection criteria, respectively. The measured paleointensities were high. The calibrated pseudo-Thellier technique was very unsuccessful, partly because the $B_{1/2ARM}$ of samples from Iceland were very low and from New-Zealand were very high. When the calculated pseudo-Thellier slopes are converted to a paleointensity the field is far lower than expected. The End-Member Modelling Approach was partly successful. The previous dataset for this model contained samples with reference paleointensities between 32 and 40μT, this range was expanded by adding the samples from Iceland and New-Zealand. The best result for the EMMA model was achieved with a 3 end-member model after removing outliers (outside 0.8-4.0) and overprints from 2.5mT for a dataset with Hawaii, Reunion, Tenerife, Iceland and New-Zealand. The model calculated an average difference in paleointensity of -0.056μT and an average absolute difference in paleointensity of 6.497μT. For the successful samples from Iceland and New-Zealand the model was able to calculate a paleointensity between 40 to 60μT, which indicates the capability of the model to calculate high paleointensities. Furthermore, the model gave accurate results for sites which were previously discarded in the pseudo-Thellier method due to an out of range $B_{1/2ARM}$. The end-members calculated with the model seem to resemble a certain iron-oxide grain distribution, the percentage of a certain end-member in a sample follows a trend with increasing Curie temperatures. This indicates there is a physical meaning behind the end-members. Because the real data-set now contains only 20 samples with high reference paleointensities and no low paleointensities, the next steps for the EMMA-technique is to expand this dataset further, to find a check to identify bad measurements and ultimately be able to apply it to samples with unknown paleointensities.

References

Aitken, M., Allsop, A., Bussell, G., & Winter, M. (1988). Determination of the intensity of the earth's magnetic field during archaeological times: Reliability of the thellier technique. *Reviews of Geophysics*, *26*(1), 3–12.

Béguin, A. (2020). Full-vector paleosecular variation curve for la réunion island, constraints on the south atlantic anomaly. *Proefschrift, Chapter 5*.

Béguin, A., Paterson, G. A., Biggin, A. J., & de Groot, L. V. (2020). Paleointensity. org: An online, open source, application for the interpretation of paleointensity data. *Geochemistry, Geophysics, Geosystems*, *21*(5), e2019GC008791.

Biggin, A. J., Perrin, M., & Dekkers, M. J. (2007). A reliable absolute palaeointensity determination obtained from a non-ideal recorder. *Earth and Planetary Science Letters*, *257*(3-4), 545–563.

Coe, R. S. (1967). The determination of paleo-intensities of the earth's magnetic field with emphasis on mechanisms which could cause non-ideal behavior in thellier's method. *Journal of geomagnetism and geoelectricity*, *19*(3), 157–179.

Day, R., Fuller, M., & Schmidt, V. (1977). Hysteresis properties of titanomagnetites: Grain-size and compositional dependence. *Physics of the Earth and planetary interiors*, *13*(4), 260–267.

De Groot, L. V., Biggin, A., Dekkers, M., Langereis, C., & Herrero-Bervera, E. (2013). Rapid regional perturbations to the recent global geomagnetic decay revealed by a new hawaiian record. *Nature communications*, *4*(1), 1–7.

De Groot, L. V., Fabian, K., Bakelaar, I. A., & Dekkers, M. J. (2014). Magnetic force microscopy reveals meta-stable magnetic domain states that prevent reliable absolute palaeointensity experiments. *Nature Communications*, *5*(1), 1–10.

De Groot, L. V., Pimentel, A., & Di Chiara, A. (2016). The multimethod palaeointensity approach applied to volcanics from terceira: Full-vector geomagnetic data for the past 50 kyr. *Geophysical Journal International*, *206*(1), 590–604.

de Groot, L. V., Béguin, A., Kosters, M. E., van Rijsingen, E. M., Struijk, E. L., Biggin, A. J., Hurst, E. A., Langereis, C. G., & Dekkers, M. J. (2015). High paleointensities for the canary islands constrain the levant geomagnetic high. *Earth and Planetary Science Letters*, *419*, 154–167.

de Groot, L. V., Dekkers, M. J., & Mullender, T. A. (2012). Exploring the potential of acquisition curves of the anhysteretic remanent magnetization as a tool to detect subtle magnetic alteration induced by heating. *Physics of the Earth and Planetary Interiors*, *194*, 71–84.

Dekkers, M. J., & Böhnel, H. N. (2006). Reliable absolute palaeointensities independent of magnetic domain state. *Earth and Planetary Science Letters*, *248*(1-2), 508–517.

Dunlop, D. J. (2002). Theory and application of the day plot (mrs/ms versus hcr/hc) 1. theoretical curves and tests using titanomagnetite data. *Journal of Geophysical Research: Solid Earth*, *107*(B3), EPM–4.

Dunlop, D. J., & Özdemir, Ö. (2001). *Rock magnetism: Fundamentals and frontiers*. Cambridge university press.

Fabian, K., & Leonhardt, R. (2010). Multiple-specimen absolute paleointensity determination: An optimal protocol including ptrm normalization, domain-state correction, and alteration test. *Earth and Planetary Science Letters*, *297*(1-2), 84–94.

Heslop, D., & Dillon, M. (2007). Unmixing magnetic remanence curves without a priori knowledge. *Geophysical Journal International*, *170*(2), 556–566.

Hill, M. J., & Shaw, J. (1999). Palaeointensity results for historic lavas from mt etna using microwave demagnetization/remagnetization in a modified thellier-type experiment. *Geophysical Journal International*, *139*(2), 583–590.

Hobden, Houghton, B., Lanphere, M., & Nairn, I. (1996). Growth of the tongariro volcanic complex: New evidence from k-ar age determinations. *New Zealand Journal of Geology and Geophysics*, *39*.

Hobden, Houghton, B. F., & Nairn, I. A. (2002). Growth of a young, frequently active composite cone: Ngauruhoe volcano, new zealand. *Bulletin of Volcanology*, *64*(6), 392–409.

Höskuldsson, Á., Óskarsson, N., Pedersen, R., Grönvold, K., Vogfjör, K., & Ólafsdóttir, R. (2007). The millennium eruption of hekla in february 2000. *Bulletin of Volcanology*, *70*(2), 169–182.

IGRF-13. (2019). 13th generation igrf - released december 2019. http://www.geomag.bgs.ac.uk/data_service/models_compass/igrf_calc.html.

Korte, M., Constable, C., Donadini, F., & Holme, R. (2011). Reconstructing the holocene geomagnetic field. *Earth and Planetary Science Letters*, *312*(3-4), 497–505.

Koymans, M. R., Langereis, C. G., Pastor-Galán, D., & van Hinsbergen, D. J. (2016). Paleomagnetism. org: An online multi-platform open source environment for paleomagnetic data analysis. *Computers & Geosciences*, *93*, 127–137.

Miller, C. A., & Williams-Jones, G. (2016). Internal structure and volcanic hazard potential of mt tongariro, new zealand, from 3d gravity and magnetic models. *Journal of Volcanology and Geothermal Research*, *319*, 12–28.

Mullender, T., Van Velzen, A., & Dekkers, M. (1993). Continuous drift correction and separate identification of ferrimagnetic and paramagnetic contributions in thermomagnetic runs. *Geophysical Journal International*, *114*(3), 663–672.

Nagata, T., Arai, Y., & Momose, K.-i. (1963). Secular variation of the geomagnetic total force during the last 5000 years. *Journal of Geophysical Research*, *68*(18), 5277–5281.

Pedersen, G., Montalvo, J., Einarsson, P., Vilmundardóttir, O. K., Sigurmundsson, F. S., Belart, J., Hjartardóttir, Á. R., Kizel, F., Rustowicz, R., Falco, N., et al. (2018). Historical lava flow fields at hekla volcano, south iceland.

Putnis, A. (1992). *An introduction to mineral sciences*. Cambridge University Press.

Readman, P., & O'reilly, W. (1972). Magnetic properties of oxidized (cation-deficient) titanomagnetites (fe, ti, _?? _) 43o4. *Journal of geomagnetism and geoelectricity*, *24*(1), 69–90.

Tauxe, L. (2010). *Essentials of paleomagnetism*. Univ of California Press.

Tauxe, L., Pick, T., & Kok, Y. (1995). Relative paleointensity in sediments: A pseudo-thellier approach. *Geophysical Research Letters*, *22*(21), 2885–2888.

Tauxe, L., & Staudigel, H. (2004). Strength of the geomagnetic field in the cretaceous normal superchron: New data from submarine basaltic glass of the troodos ophiolite. *Geochemistry, Geophysics, Geosystems*, *5*(2).

Thébault, E., Finlay, C. C., Beggan, C. D., Alken, P., Aubert, J., Barrois, O., Bertrand, F., Bondar, T., Boness, A., Brocco, L., et al. (2015). International geomagnetic reference field: The 12th generation. *Earth, Planets and Space*, *67*(1), 1–19.

Thellier, E. (1959). Sur l'intensité du champ magnétique terrestre dans le passé historique et géologique. *Ann. Geophys.*, *15*, 285–376.

Thordarson, T., & Larsen, G. (2007). Volcanism in iceland in historical time: Volcano types, eruption styles and eruptive history. *Journal of Geodynamics*, *43*(1), 118–152.

Valet, J. P., Herrero-Bervera, E., Carlut, J., & Kondopoulou, D. (2010). A selective procedure for absolute paleointensity in lava flows. *Geophysical research letters*, *37*(16).

van Grinsven, L. (2020). End-member modeling analyses (emma) of pseudo-thellier style experiments to derive absolute paleointensities from lavas. *Guided Research*.

Wilson, C., Rogan, A., Smith, I., Northey, D., Nairn, I., & Houghton, B. (1984). Caldera volcanoes of the taupo volcanic zone, new zealand. *Journal of Geophysical Research: Solid Earth*, *89*(B10), 8463–8484.

Yu, Y., Dunlop, D. J., & Özdemir, Ö. (2003). Are arm and trm analogs? thellier analysis of arm and pseudo-thellier analysis of trm. *Earth and Planetary Science Letters*, *205*(3-4), 325–336.